Final Technical Report

Internal Short Circuits in Lithium-Ion Cells for PHEVs

Award Number: DE-EE0003378

Recipient: TIAX LLC

35 Hartwell Avenue

Lexington, MA 02476

Principal Investigators: Dr. Suresh Sriramulu

Dr. Richard Stringfellow

1. Introduction

Development of Plug-in Hybrid Electric Vehicles (PHEVs) has recently become a high national priority because of their potential to enable significantly reduced petroleum consumption by the domestic transportation sector in the relatively near term. Lithium-ion (Li-ion) batteries are a critical enabling technology for PHEVs. Among battery technologies with suitable operating characteristics for use in vehicles, Li-ion batteries offer the best combination of energy, power, life and cost. Consequently, worldwide, leading corporations and government agencies are supporting the development of Li-ion batteries for PHEVs, as well as the full spectrum of vehicular applications ranging from mild hybrid to all-electric.

However, concerns regarding the safety of Li-ion batteries could severely limit their use in PHEVs, and undermine the prospects for realizing the appealing benefits of PHEVs. Highly publicized safety incidents and the ensuing widespread recalls of Li-ion batteries (used in laptops and cell phones) have elevated such concerns. In these safety incidents, called field-failures, Li-ion batteries operating under otherwise normal conditions undergo what appear to be spontaneous thermal runaway events with violent flaming and extremely high temperatures. These field failures cause significant damage to cells, packs and devices, and sometimes to their surroundings. Because a typical PHEV pack would be significantly larger than a typical laptop pack (~200 times on an energy basis), field-failure in a PHEV pack could inflict far greater damage than would be the case for a similar failure of a laptop pack and, with roughly 75 cells in a PHEV pack, would occur far more frequently than in laptops, which generally have 6 – 10 cells. Indeed, there have been recent instances[1] of batteries in PHEV and EV automobiles that have spontaneously experienced thermal runaway under normal operation.

Although it is well-recognized that commercial viability of Li-ion technology in PHEVs is dependent on avoiding spontaneous occurrence of such incidents on board vehicles, it is less well-recognized that the safety technologies currently employed in commercial Li-ion batteries for portable electronic applications are inadequate. For example, the many millions of cells recalled in the last few years due to safety incidents all came from production lots that passed all industry-standard safety tests. Furthermore, there are currently a variety of standard safety-related technologies to guard against abuse of the Li-ion battery; electronic controls, current interrupt and positive temperature coefficient devices, shutdown separators, etc., are intended to counter potential hazards due to inadvertent overcharge, failure of protection circuits, exposure to high temperatures, external short circuits, etc. However, multiple safety incidents have occurred despite the presence of these technologies (in their fully functional state) in cells and packs. The reason for this apparent conundrum is discussed later in this report, but essentially relates to the fact that these safety components are not designed to guard against the slowly developing internal short. Furthermore, there is no adequate predictive test to identify susceptibility of a cell to the type of field-failure and internal short circuit that presents a basic safety issue for Li-ion.

Internal shorts from metal particle contamination have been identified as the overwhelming reason for thermal runaway in safety-related field-failures. Recent work done at TIAX has identified the mechanism of internal short formation from the presence of metal particles in cells. Essentially, metal particles present in/on the cathode of Li-ion cells can dissolve under normal operating conditions, plate on the anode, and grow back as a dendrite to contact the cathode.

However, relatively little is known about the progression to thermal runaway following internal shorts. Gaining such an understanding is crucial to identifying approaches to reduce the propensity for thermal runaway from internal shorts.

In this project, using a combination of well-defined experiments, custom designed cells and simulations, we have improved the understanding of the process by which a Li-ion cell that develops an internal short progresses to thermal runaway. Using a validated model for thermal runaway, we have explored the influence of environmental factors and cell design on the propensity for thermal runaway in full-sized PHEV cells. We have also gained important perspectives about internal short development and progression; specifically that initial internal shorts may be augmented by secondary shorts related to separator melting. Even though the nature of these shorts is very stochastic, we have shown the critical and insufficiently appreciated role of heat transfer in influencing whether a developing internal short results in a thermal runaway. This work should lead to enhanced perspectives on separator design, the role of active materials and especially cathode materials with respect to safety and the design of automotive cooling systems to enhance battery safety in PHEVs.

2. Background on Li-ion Safety

Li-ion battery safety concerns arise from the fact that, given suitable triggers, the organic solvent-based electrolytes employed in today's lithium-ion cells are capable of undergoing highly exothermic reactions with the charged electrodes in a violent thermal runaway event. The potential for this sort of safety incident has also impeded the implementation of the highest energy Li-ion cell chemistries, with lower energy content Li-ion chemistries being commercialized instead.

All safety incidents can usefully be considered in terms of three broad categories that recognize common characteristics of the physics involved in cells' response to triggers that can (if unchecked) lead to thermal runaway. It is useful to recognize these largely distinct categories because potential strategies to protect against each class of safety event involve similarities dictated by these physics. These three categories are: (1) simple abuse, in which cell temperature is essentially homogeneous (e.g., exposure to high temperature, forced overcharge), (2) impact/mechanical intrusion in which a highly non-homogeneous temperature distribution results from sudden formation of one or more hard shorts, and extremely rapidly progresses to thermal runaway, and (3) 'grown-in' internal shorts, in which rare manufacturing defect-caused internal shorts can mature to the stage at which a hot spot forms and eventually results in a thermal runaway.

In commercial batteries, the first category of trigger is generally controlled by a variety of cell components, sensors and the battery management system (BMS). The second category of failures has been actively investigated over several years by battery companies and other end-users. Recently, at TIAX we have developed an exciting solution to enhance the safety of the Li-ion cell to this class of trigger. The third class of trigger, the 'grown-in' internal short-circuit, has not received much attention, despite the fact that it is the most insidious type of safety failure because of its lack of predictability and because it is not protected against by internal cell components such as PTCs or CIDs. For several years, TIAX has been developing experimental techniques and simulation tools to understand this type of trigger and the factors that control the progression to thermal runaway. The insights from such work have allowed TIAX to develop an exciting technology to detect internal shorts at a very early stage before they pose a thermal runaway risk. Such early-stage detection can allow a wide range of intervention techniques that are under evaluation at TIAX, to minimize the risk of thermal runaway.

However, additional work is needed to understand the progression towards thermal runaway following an initial internal short-circuit. This work aims to enhance the understanding of thermal runaway of Li-ion cells by using a combination of experiments and modeling.

2.1. Reasons for Li-ion Cell Safety Concerns

Li-ion safety events do not take place spontaneously; they occur as a consequence of exposure of a cell to a "trigger". Li-ion cells achieve high energy density by employing highly energetic active and inactive materials. However, the active materials, when exposed to suitable "triggers", can experience exothermic reactions. When the rate of heat release from such exothermic reactions exceeds the rate at which heat can be removed from a Li-ion cell, thermal runaway ensues, typically with smoke, sparks and flame, and sometimes with explosive rupture

of cell casings. Figure 1 summarizes the exothermic reactions that can be involved in a thermal runaway event.

Process	Temperature Range (°C)	Energy release[1]
Decomposition at anode	80 -120 150 - 300	~ 400 J/ g-anode[1,2] ~ 1200 J/g-anode[1,2]
Decomposition at cathode	150 - 300	~ 1300 J / g-cathode[2]
Self-reaction of salt with solvent	250 - 400	~ 900 J/g electrolyte[3]
Complete combustion of solvent[2]	Auto-ignition temperature ~ 450	~ 18 kJ / g solvent
Complete combustion of carbon[2]	Auto-ignition temperature ~ 200	33 kJ / g carbon

[1] Approximate values estimated from DSC and ARC testing of cell components: charged anodes and cathodes, and typical electrolyte compositions;
[2] There is insufficient oxygen available inside an 18650 cell to effect complete combustion of the solvent or carbon. However, if vented at high temperatures or vented in the presence of an ignition source the solvent and carbon can burn outside the cell.

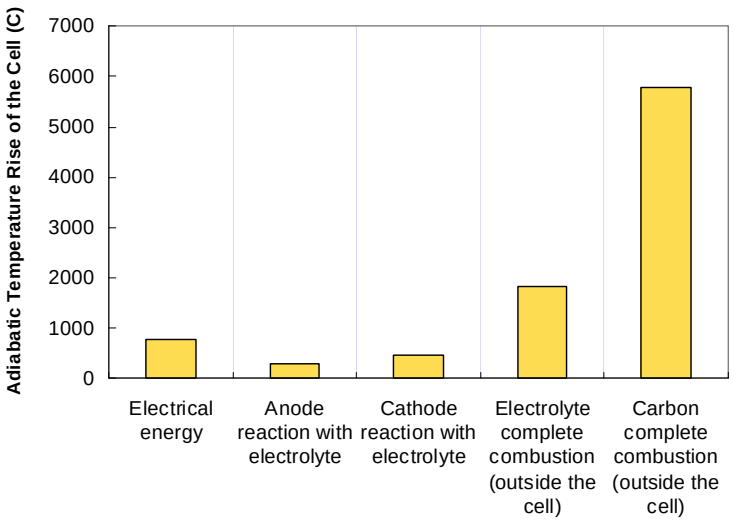

Figure 1: Summary of sources of exothermic heat release in a Li-ion cell. The table on the left lists the main exothermic reactions, the temperature range over which these reactions initiate, and the expected amount of heat release in an 18650 cell. The plot on the right quantifies the amount of heat release in terms of the adiabatic temperature rise of a typical Li-ion cell.

The table on the left of Figure 1 gives the typical range of temperatures for onset of the exothermic reactions in a typical Li-ion cell[2], while the right-hand chart quantifies the heat release in terms of the adiabatic temperature rise of the cell. Exothermic anode/electrolyte and cathode/electrolyte reactions together provide comparable heat release to the electrical energy content of the cell, which by itself is sufficient to raise the cell temperature to > 700ºC. Complete combustion of the organic solvent outside the cell can provide much more heat. Note that even in cells with metal oxide cathodes, the amount of oxygen available from cathode decomposition is only a third of that needed for complete combustion of the electrolyte, indicating that a majority of the solvent combustion will occur outside the cell (consistent with experimental observations). Finally, and leaving aside the possibility of potential thermite reactions, the combustion of the carbon from the anode and conductive carbon additives can provide even greater heat release. The potential for such great heat release is the basis for safety concerns and the reason that Li-ion safety triggers must be understood and addressed.

One of the triggers that has not received much attention is the ‘grown-in’ internal short trigger responsible for the safety incidents discussed in the introduction. On rare occasions, Li-ion cells experience thermal runaway during otherwise “normal” charge/discharge cycles because of internal short-circuits; we term such incidents “field-failures.” Even though such incidents are rare, the potential consequences can be very serious. Safety technologies currently employed in Li-ion cells, such as PTCs, CIDs, shut-down separators, etc., have not prevented thermal runaway due to internal shorts in commercial Li-ion cells. Development of new safety

technologies is hindered by the rarity of field-failures in Li-ion cells, and the current incomplete understanding of field-failures.

In the case of the ‘grown-in’ internal short trigger, a short circuit is formed within the cell as a subsequent consequence of certain manufacturing defects, or metal particle inclusions. Note that not all metal particles present in a cell will result in thermal runaway. When such an internal short is created, the cell discharges through the internal short, resulting in a hot-spot. The active materials in this hotspot will undergo exothermic reactions (as indicated in Figure 1), further contributing to the energy release in this region of the cell. Under the right conditions of heat generation in the hotspot and heat removal from the hotspot and the cell, thermal runaway occurs.

At TIAX, we have studied the initiation and growth of these internal short circuits using a combination of experimental measurements and simulations. Based on insights from this work, we have recently developed a non-invasive technology to detect the initiation and growth of incipient internal short circuits so that suitable intervention approaches can be deployed. The phenomena leading to thermal runaway from such short circuits are not completely understood at this point primarily because well-characterized experimental thermal runaway data have not been available. Understanding how cell design parameters and environmental conditions influence thermal runaway is critical to developing cell-level and pack-level technologies that can enhance the safety of Li-ion cells with respect to the ‘grown-in’ internal short trigger.

Several researchers have attempted to improve the understanding of thermal runaway of Li-ion cells through simulations. While such efforts have provided insightful information, few models have been compared to experimental thermal runaway data, thereby limiting the usefulness of the predictions from such models and limiting the ability to explore the basis for variations in predictions of these models. Part of the reason for this gap is the absence of well-characterized experimental data on thermal runaway of L-ion cells. Unfortunately, most of the experimental data on thermal runaway of Li-ion cells in the literature have not been developed under conditions of controlled heat transfer. As we shall show in this work, the heat transfer rate at the cell surface plays a crucial role in determining the outcome in (potential) thermal runaway experiments. Moreover, in most experiments that employ commercially available cells, the cell internal parameters — properties of materials, etc. — could not be accurately estimated.

In this program, we used well-characterized experimental data to calibrate parameters of an FEA model for thermal runaway, and then used the calibrated model to assess the implications of internal short-induced thermal runaway in large-format PHEV cells. Details of the FEA model employed in this work are provided in Section 6.1.

3. Project Objectives and Approach

3.1. Objectives

The overall objectives of this project were to: (1) model characteristics of internal shorts in lithium-ion cells that result in thermal runaway and characterize threshold conditions for these events; (2) verify model predictions in lithium-ion cells; and (3) analyze opportunities for detecting imminent safety-related field failures and preventing their occurrence. This program aimed to identify, through modeling and experiments, the conditions under which internal short circuits in Li-ion cells will induce thermal runaway and identify design factors that can reduce propensity for thermal runaway.

Specific technical objectives were to:

- Develop guidelines that will enable the development of technologies for a safe battery pack.
- Establish a facility for fabricating Li-ion cells to: (1) study the effect of cell materials and cell design parameters on thermal runaway; (2) compare results of cell testing under controlled conditions to TIAX's Li-ion cell FEA model predictions; and (3) validate the FEA model.
- Establish an experimental facility that permits testing of the efficacy of technologies developed to mitigate safety incidents that occur in the field.
- Select and test approaches to enhance Li-ion battery safety using validated model and experimental data.

3.2. Approach

Our overall approach to developing guidelines for safe PHEV pack design focused on preventing the first cell from experiencing thermal runaway, thereby not allowing cascading processes to occur. We employed an FEA model to determine the conditions under which thermal runaway of PHEV-size cells occurs and can be suppressed. The parameters of the FEA model were first calibrated using thermal runaway data collected on custom-designed 18650 cells. Key parts of this approach are summarized below:

- 18650 cells were custom-designed and built on our cell prototyping line with a range of design variations (including active materials) for thermal runaway tests.
- Thermal runaway was induced by introducing a miniature heater into the center of the cell through a tiny hole drilled through the bottom of the can. This approach allowed us to experimentally simulate local, spot heating of the cell, akin to what transpires when an internal short occurs.
- Thermal runaway data were obtained under a range of carefully controlled external heat transfer conditions. Thermal runaway testing under controlled heat transfer conditions was critical for calibrating model parameters. A wind-tunnel was designed and constructed in order to enable testing under controlled external heat transfer conditions. In addition, the progression to thermal runaway was quenched in experiments and tear-down of the cells subsequently provided significant insights into the progression to thermal runaway.

- Separate measurements of component properties (such as the kinetics of anode/cathode exothermic heat release) were obtained and used as inputs to the model.
- Model parameters were calibrated by fitting thermal runaway data under a wide range of conditions. This fitting/comparison to experimental thermal runaway data yielded a host of insights into the progression to thermal runaway from internal shorts, with implications for the design of safer cells.

The FEA model with calibrated parameters was then used to assess the factors responsible for thermal runaway in large-format PHEV cells. Sensitivity analysis with the FEA model provided significant insights into the cell-design and environmental factors that influence thermal runaway.

4. Custom Cell Fabrication Facility

A Li-ion cell prototyping facility was constructed in order to fabricate custom-designed cells to probe the influence of cell design on propensity for thermal runaway, and use such custom-designed cells to calibrate/validate our FEA model. This chapter describes the facility and its capabilities.

4.1. Facility capabilities

The equipment in the facility, and the layout itself, was specified with flexibility of cell design in mind:

- *Cell shape:* The facility can fabricate cylindrical cells (18650 or 26650 formats), wound prismatic or stacked prismatic cells.
- *Cell size:* We have successfully fabricated 18650 cells with > 2 Ah capacity (with electrode loadings corresponding to PHEV designs) and specific energy of ~200 Wh/kg and > 2.5 Ah capacity (with electrode loadings corresponding to EV designs) with specific energy of ~250 Wh/kg. Stacked prismatic pouch cells with capacity of ~3 Ah have also been successfully fabricated. Even larger cell sizes (e.g., 10 Ah) can also be fabricated.
- *Cell components:* Cells can be fabricated with a wide range of active and inactive components. We have successfully fabricated and tested cells with NCA or NCM cathode material, and multiple grades of graphite. We have also evaluated, in a separate project, the impact of ceramic coatings on separators with respect to their effect in nail penetration testing. Other cell-level modifications were found to be successful in ensuring a benign outcome in nail penetration tests.
- *Modification of cells to enable safety tests:* Cells fabricated at TIAX can also be purposely modified during fabrication for safety studies. We have demonstrated successful internal short formation from metal particles implantation by deliberately incorporating metal particles into the electrodes prior to cell formation. We have also inserted miniature heaters into the cells prior to formation so that the cells can be internally heated to simulate a hot spot that would occur as a result of an internal short circuit.

4.2. Equipment and Layout

Equipment was specified and purchased from reputable vendors in the US, Korea and Japan. TIAX staff participated in Field Acceptance Trials (FAT) at vendor sites prior to equipment delivery and approval at TIAX. Representatives from the equipment vendor companies for the cell fabrication equipment visited TIAX for assistance with equipment installation, equipment commissioning, and training of TIAX staff to use the equipment.

TIAX facilities were modified to accommodate the cell fabrication facility. Dedicated laboratory space was made available for the prototyping facility, the HVAC systems at TIAX were modified to accommodate the exhaust from the coater, and electrical systems were modified to accommodate the power requirements of the various pieces of equipment.

A floor plan of the prototyping facility is shown in Figure 2 and photographs of the key pieces equipment are shown in Figure 3. The facility comprises a total of three rooms:

- a mixing room that houses a double-planetary, double-disperser mixer which is capable of handling electrode slurries (either water-based or NMP-based) with a wide range of viscosities;
- a coating room that houses a reverse-comma coater with a 5 m long heating zone, that is capable of intermittent coatings (for either water-based or NMP-based slurries) and can prepare electrodes with a wide range of electrode loadings;
- a dry room (-40ºC dew point), that houses the remaining equipment needed for cell fabrication: electrode slitter, electrode calendaring machine, semi-automatic winder with edge-position control to prepare high-quality wound (cylindrical or prismatic) cells, a crimping machine, a grooving machine, an electrolyte filling machine, and spot welders. Not shown is large dehumidifying unit for the dry room, which was located outside the building.

In addition to the equipment shown here, several custom-fixtures and holders were designed and fabricated at TIAX to facilitate cell fabrication.

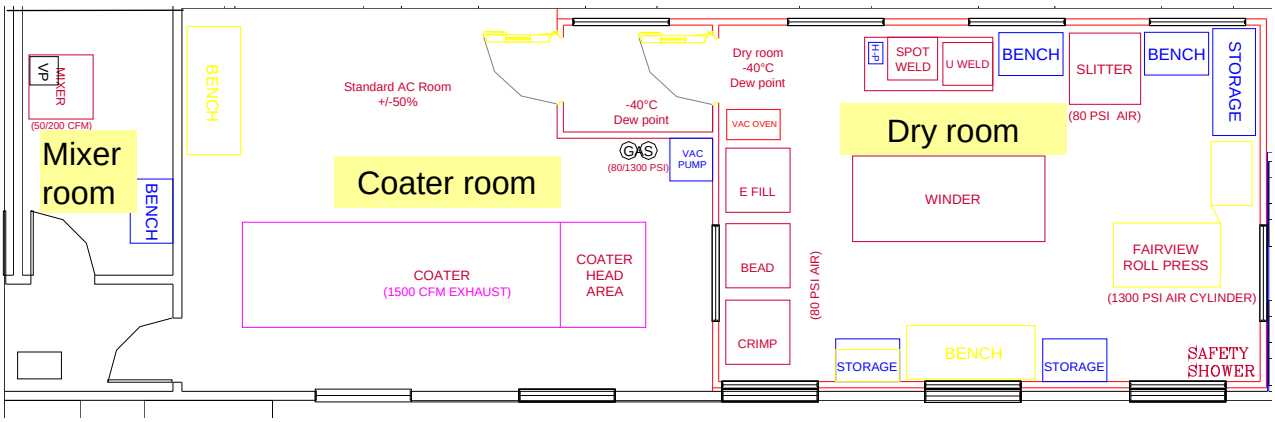

Figure 2: Schematic of the layout of the Li-ion cell fabricating facility at TIAX.

Figure 3: Photographs of the mixer (left) and coater (right)

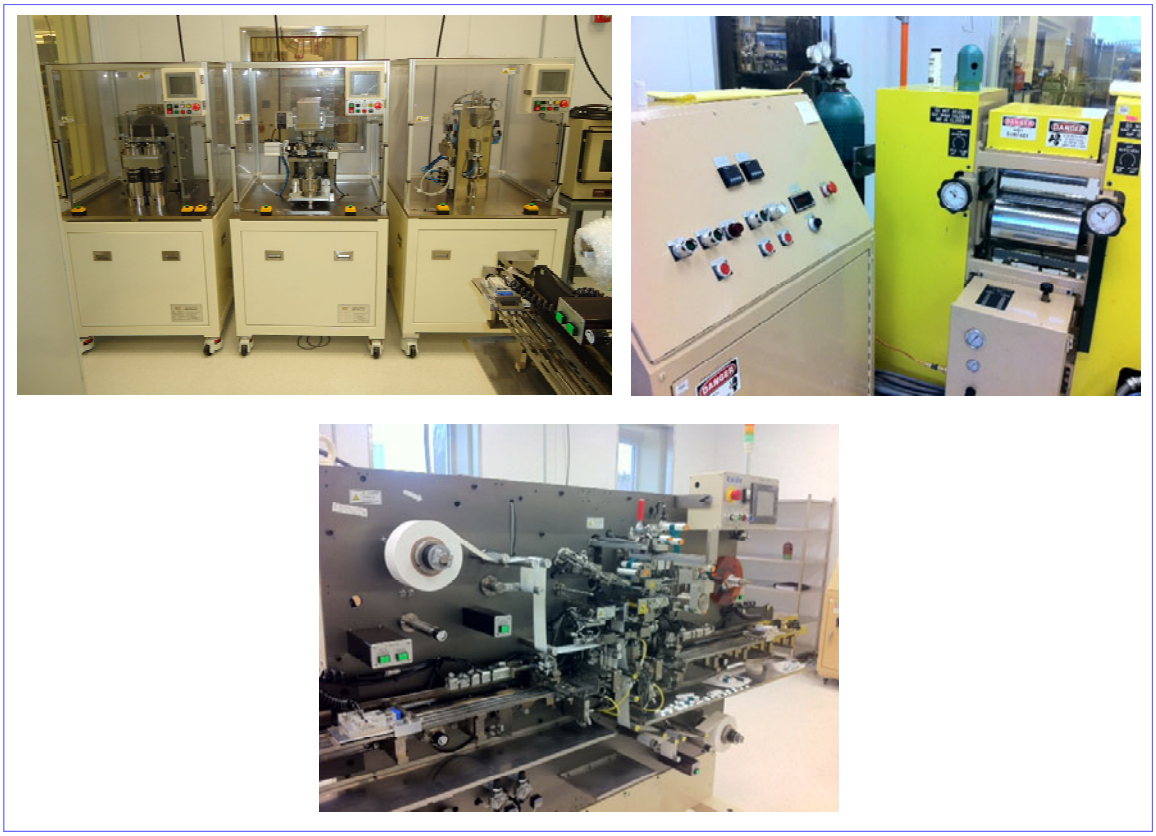

Figure 4: Photographs of equipment housed in the dry room. Top left photograph shows the grooving machine, electrolyte filler, and crimping machine. Top right photograph shows the calendaring machine; and bottom photograph shows the semi-automatic winder.

4.3. Cell Performance

Cells with PHEV electrode designs were successfully fabricated. For these cell fabrication trials, we employed commercially-available cathode, anode, separator, and electrolyte materials. Sample cycle life data for NCA-based cells fabricated in our facility are shown in Figure 5, indicating that the cells are of very good quality. Achieving consistently good cycle life is only possible with good quality cell fabrication techniques. Achieving this level of cell build quality required several iterations with successive build quality improvements in each iteration. For example, the initial rounds of cell builds had more than a 60% failure rate because of soft internal short circuits. However, improved electrode tolerances and better housekeeping virtually eliminated soft shorts, and we now obtain excellent reproducibility of cell performance.

Each cell build was preceded by a detailed design of the cell using our proprietary cell engineering model. Electrodes were fabricated and calendared according to the dimensions prescribed by the model in order to achieve the design capacity. The model incorporates all aspects of the cell construction necessary to accurately predict cell capacity, including the diameter of the central mandrel, the amount of bare foil at the center and the periphery, the thicknesses and widths of the electrodes, current collectors, and separators, the length of the initial separator winding and the length of separator at the outside of the jelly roll, can internal

dimensions, etc. The measured capacity of the fabricated cells closely matched the predicted values from the cell engineering model, thereby repeatedly validating the engineering model.

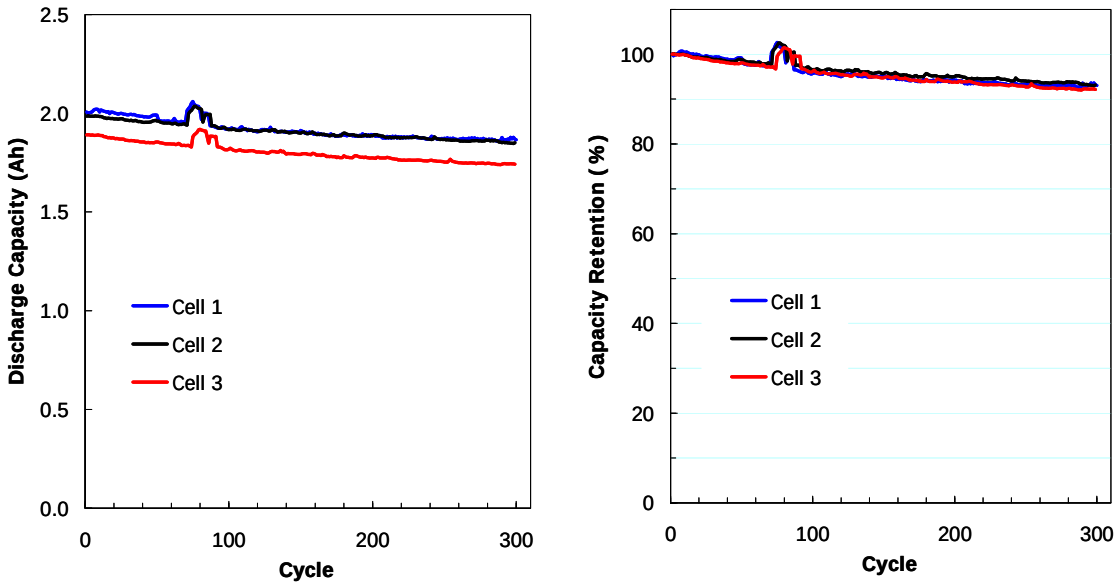

Figure 5: Example of cycling performance of 18650 cells fabricated at TIAX. These cells incorporated commercially available components for cathode (NCA), anode (graphite), separator, and electrolyte. The NCA cathode electrode had active material loading of ~15 mg/cm2 per side, formulation of 94:3:3 (AM:cc:PVdF), and density of ~ 3.05 g/cc. The nominal anode to cathode ratio was ~1.2. The graphite anode electrode had a formulation of 96:4 (AM:binder), and density of 1.6 g/cc. The cycling data reported here are for cycling between 4.2 V and 2.75 V, with C/2 charge and 1C discharge.

4.4. Baseline Cell Design for Thermal Runaway Experiments

18650 cells were fabricated on the prototyping line for thermal runaway experiments. The active materials, electrode design and information, and initial performance of the baseline cells are summarized in Table 1.

Table 1: Summary of cell design parameters for the baseline 18650 cells used for thermal runaway experiments

Parameter	Target Values
Cathode material	NCA
Cathode electrode design	Active material loading: 16 mg/cm^2 Electrode formulation: 94:3:3 (AM:cc:PVdF) Electrode density: 3.05 g/cc
N:P ratio	1.2 – 1.25
Anode material	Graphite
Anode electrode design	Active material loading: 11 mg/cm^2 Electrode formulation: 96:4 (AM:binder) Electrode density: 1.67 g/cc
Cell discharge capacity	1.9 Ah (C/5) discharge, 4.2 V to 2.75 V

5. Thermal Runaway Data on TIAX-Fabricated Li-ion Cells

We developed a method to reliably create thermal runaway in 18650 Li-ion cells. The method involved placement of a miniature heater into the core of the 18650 cell to simulate localized heating from an internal short circuit, and is described in greater detail below.

Initially, we tried to induce thermal runaway of TIAX-fabricated cells by placing metal particles into the cells during the cell fabrication, a method we had previously developed and applied successfully over several years of work using commercial 18650 cells. However, we found that while we could reliably create internal shorts in the cells with this approach during normal charge/discharge operation of cells, obtaining thermal runaway with this method required the perfect conditions of internal short resistance and external heat transfer coefficient. Such conditions could not be obtained as consistently as we required for this project. Given the highly stochastic nature (essentially the resistance) of internal short formation from metal particles, we decided to use the heater method as a more reliable approach to creating internal shorts, particularly for generating thermal runaway data for model validation.

5.1. Experimental Methods and Set-Up

5.1.1. Heater Method

We developed a heater method to reliably induce thermal runaway in Li-ion cells under controlled conditions. In this method, a miniature heater is inserted into a Li-ion 18650 cell through a tiny hole drilled at the bottom of the can as shown in Figure 6. The heat dissipation through the heater can be controlled through a variac. Heaters were designed and constructed at TIAX.

By varying the heat dissipation, the thermal properties of the cell can be estimated by fitting to the model. An example is shown in Figure 7 and Figure 8. Figure 7a shows the position of the heater within the core of the cell, and the positions of thermocouples inside and outside the cell. A completely discharged cell was employed to eliminate the possibility of thermal runaway in this test. Figure 7b shows sample data of the core and external temperature as a function of heater power. At each heater power, the temperatures were allowed to reach steady state before the power was subsequently increased. At steady state, the rate of heat removal from the surface equals the rate of heat input from the heater. Using this approach, the surface heat transfer coefficient can be accurately estimated. Moreover, by fitting the rate of rise of core and surface temperatures with the FEA model, the thermal conductivity and specific heat values can also be estimated. For the data shown in Figure 7b, when the heater power is increased from 1 W to 4 W, the core temperature increases from about 50ºC to 200 ºC, whereas the surface temperature increases only from 30ºC to 60ºC, illustrating the complex balance between the cell internal thermal conductivity and the heat transfer from the cell surface.

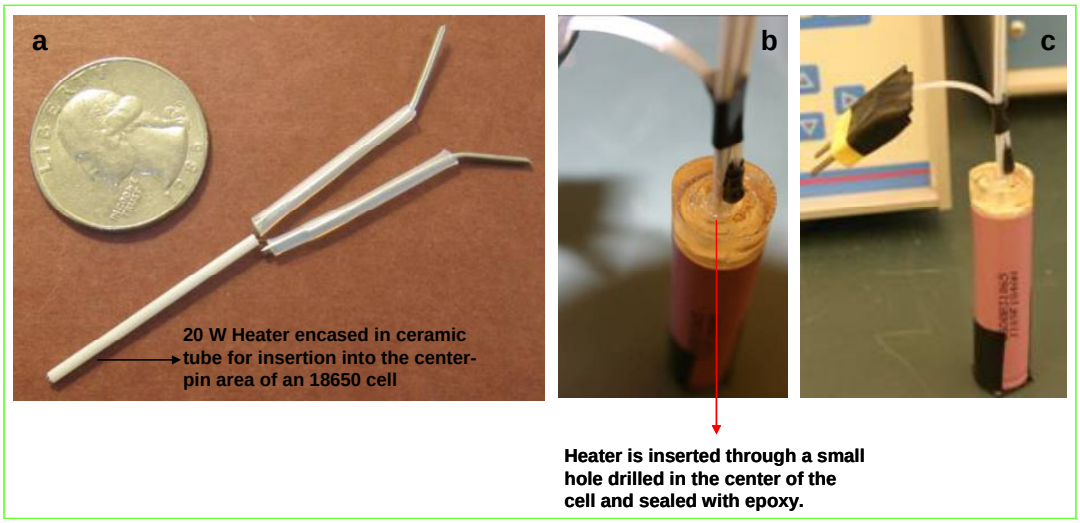

Figure 6: Photographs depicting the heater method. (a) a 20 W heater sheathed in ceramic; (b) and (c) an 18650 cell with heater inserted.

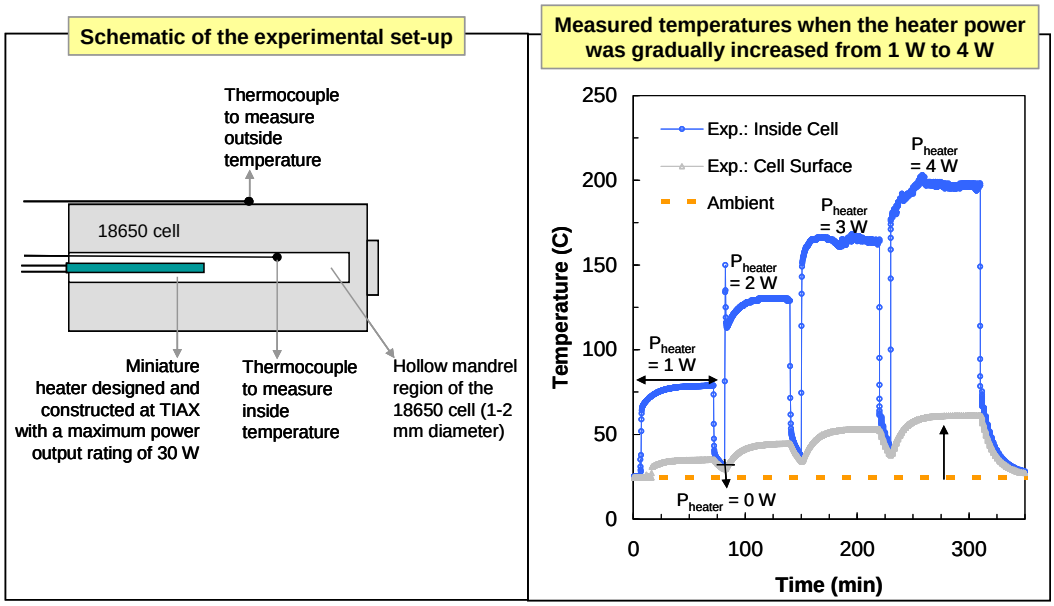

Figure 7: (a) Schematic of experimental set-up and (b) thermocouple data for characterizing cell thermal properties.

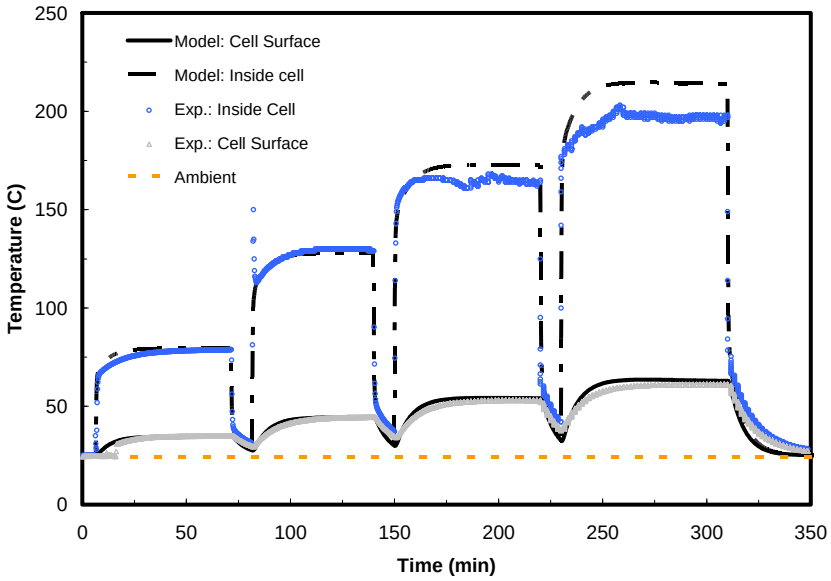

Figure 8: Example of model fit to the experimental data from Figure 7.

5.1.2. Set-up for Controlled Heat Transfer Experiments

Our previous work has shown that the surface heat transfer coefficient plays a major role in the progression to thermal runaway. In order to control the external heat transfer coefficient during thermal runaway, we designed and built a wind tunnel capable of providing stable and known heat transfer conditions for such tests. Photographs of the wind tunnel are shown in Figure 9. The top photograph shows the complete wind tunnel as originally designed and built. The bottom figure shows a close-up of the chamber within the wind tunnel that houses the 18650 cells used in the thermal runaway tests. Two 18650 cells can be seen — a test 18650 cell and reference 18650 cell — suspended using thin wires from the ceiling of the test chamber. This arrangement minimized dissipation of heat through the wires as well as disruption of the air flow field around the cell, which was important to obtain a near-uniform heat transfer coefficient around the cell. These cells had thermocouples attached to their respective surfaces to measure the skin temperature.

The film heat transfer coefficient on the cell surface measured as a function of the air velocity in the wind tunnel is shown in Figure 10. To characterize the heat transfer coefficient, the heater method was used. Essentially a fully discharged 18650 cell with an implanted heater was suspended within the chamber. The cell surface temperature was measured as a function of the heater input power at steady state, as shown in Figure 7. Given that at steady state the rate of heat output from the cell equals the rate of heat input from the cell (which is known), and knowing the cell surface temperature (measured), the heat transfer coefficient could be easily calculated. Similar measurements were performed over a wide range of air flow settings and heater input powers. In these measurements, we found that the length of the wind tunnel could be reduced without affecting the air velocity / heat transfer coefficient relationship. The results of these measurements, as shown in Figure 10, indicate that a significant increase in surface heat transfer rates can be achieved through relatively modest levels of air flow.

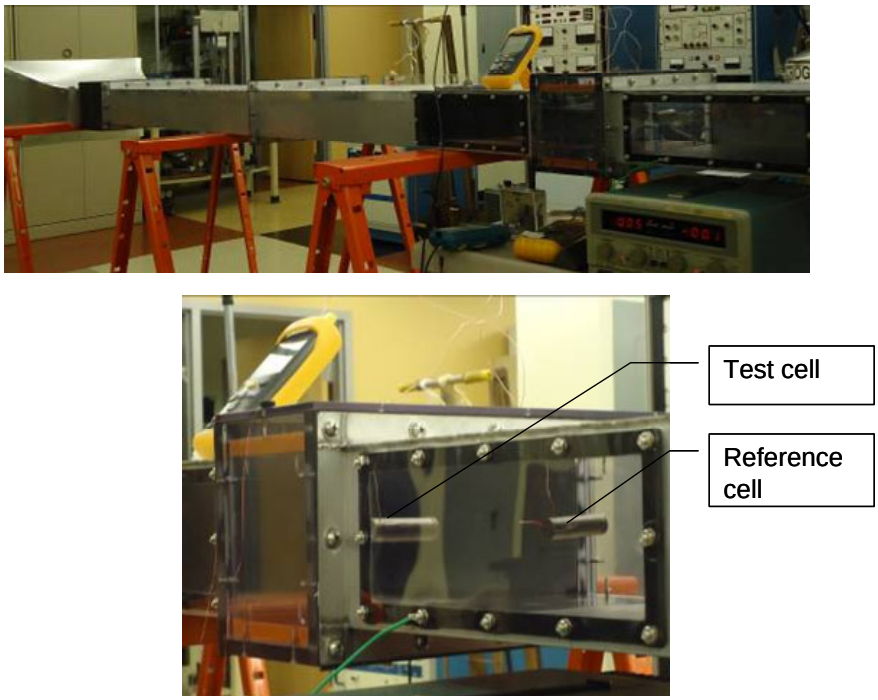

Figure 9: Photographs of the experimental set-up showing the chamber for controlling the heat transfer coefficient during thermal runaway experiments. The top photograph shows a wind tunnel purpose-built for controlled heat transfer coefficient measurements. The bottom photograph shows a close-up of the chamber that houses two 18650 cells – a test cell (fully charged) and a reference cell (fully discharged). The 18650 cells (with inserted heaters) are suspended from the ceiling of the test chamber by thin wires.

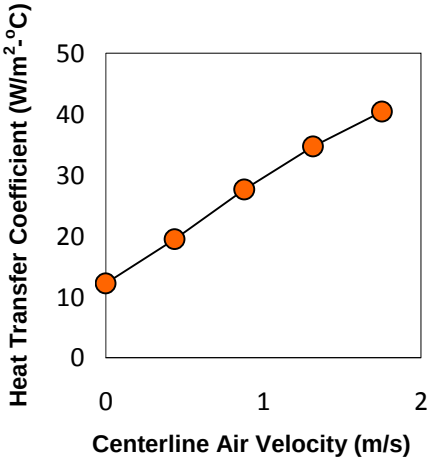

Figure 10: Sample film heat transfer coefficient for an 18650 cell as a function of the flow rate of air measured in the wind tunnel shown in Figure 9.

5.2. Experimental Thermal Runaway Data

The heater method and test chamber described in the previous sections were used for thermal runaway measurements of Li-ion 18650 cells fabricated at TIAX under conditions of controlled surface heat transfer coefficient. For thermal runaway measurements, the test cell was charged to 4.2 V and the reference cell was fully discharged. The heater method was used to heat both the

test and reference cells from the inside, with the same power input. The desired heat transfer coefficient was dialed-in by controlling the air flow. The wind-tunnel with reduced length was mounted into a walk-in hood at TIAX for the thermal runaway experiments. This section summarizes the key experimental data that were then used for model validation described later in Section 6.

The experimental procedure for initiating thermal runaway was as follows: 18650 cells with NCA cathode and commercial graphite anode were prepared according to the design described in Section 4.4. After electrochemical formation of the cells, heaters were implanted into the cells as described in Section 5.1. A fully charged cell (referred to as the 'live' cell) and a fully discharged reference cell (referred to as the 'dead' cell) were placed in the heat transfer chamber as described in Section 5.1. At time t = 0, the power to the heaters in the live cell and the dead cell was simultaneously turned on and the surface temperatures of the cells were monitored until the end of the experiment. In addition to the cell surface temperatures, the terminal voltages across the cells were also measured.

Sample thermal runaway data measured for TIAX-fabricated NCA cells are displayed in Figure 11. In this experiment, the heater power was set to 10 W and the heat transfer coefficient was set to 15 W/m^2-K. The heater was turned on at time t = 0, and turned off at ~900 s so that the cell would gradually cool down under air flow, and thermal runaway occurred at ~700 s. At time t = 0, the surface temperatures of the cells are at room temperature, but increase slowly as the cell is heated from the inside at 10 W. As the surface temperature of the live cell approaches ~110ºC, there is a sudden drop in the cell terminal voltage and the cell experiences thermal runaway as evidenced by a sharp rise in temperature. In contrast, the reference (dead) cell temperature does not exceed 110ºC, although it was heated at the same rate as the live cell.

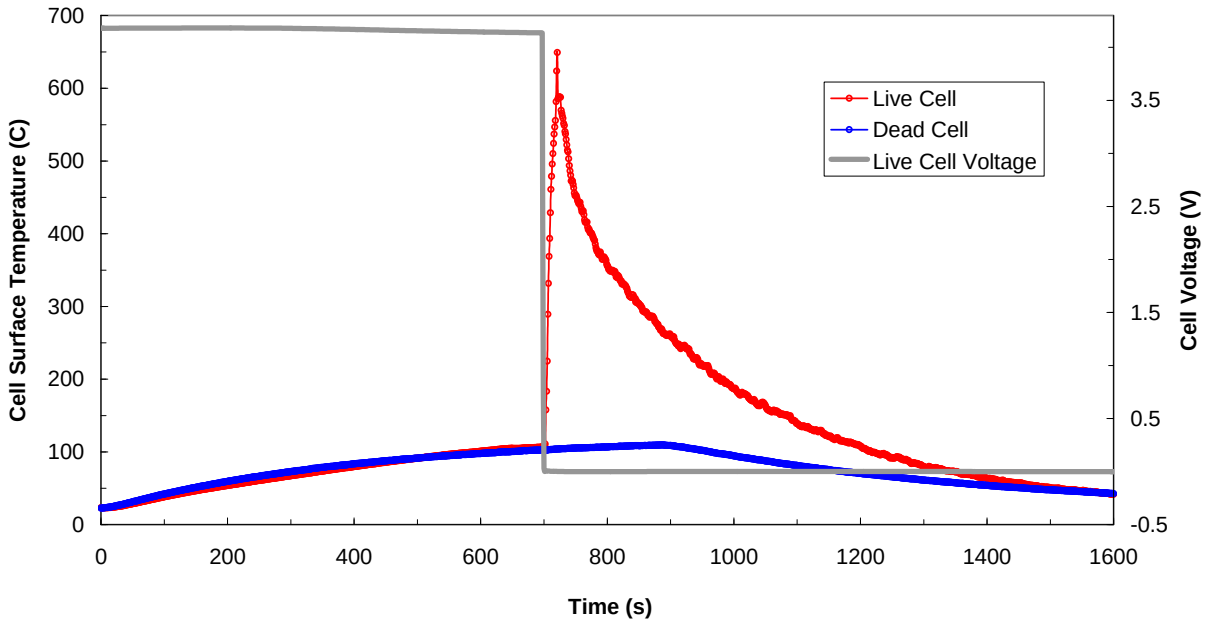

Figure 11: Example of thermal runaway data from measurements in the heat transfer chamber. The heater power input was set to ~10 W at time t=0. The air flow rate was set to achieve a surface heat transfer coefficient, h, of 15 W/m^2-K. The 18650 cell used in this experiment incorporated commercial NCA and graphite anodes and was based on the baseline cell design described in Section 4.4.

Figure 12 shows a close-up of the live and dead cell temperatures for the data from Figure 11. As can be seen, the live cell temperature rises sharply during thermal runaway, whereas the dead cell temperature continues to rise gradually because its sole source of heat remains the power input from the inserted heater. It is noteworthy that the rate of temperature increase for the live and dead cells are similar until ~700 s, when thermal runaway occurs in the live cell, suggesting that prior to the thermal runaway the additional heat release from the anode and cathode decomposition reactions (in the live cell) did not significantly contribute to the progression to thermal runaway, and obviously that simple increase in temperature is not a reliable indication of impending thermal runaway. It is also noteworthy that the cell surface temperature was only ~110 ºC when there was a sharp drop in cell voltage and thermal runaway occurred. This temperature is lower than both the temperature for separator shutdown (~130 ºC) and the temperature at which major cathode decomposition reactions occur (~200 ºC). These observations show that conventional thinking regarding material stability or separator shut down does not directly relate to cell thermal runaway when highly inhomogeneous temperature distributions are present. As we shall discuss in Section 6, the rapid drop in cell voltage is likely due to separator melting in the vicinity of the heater (representing, by implication, a hot spot), causing an internal short and significant secondary power dissipation through this short.

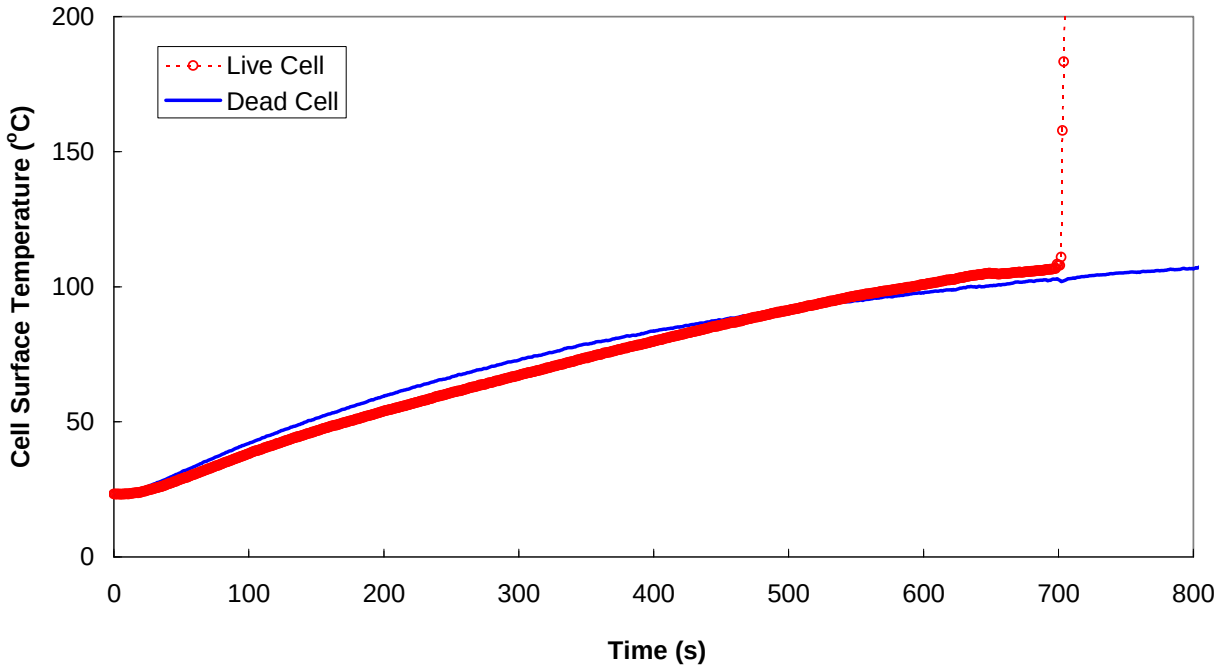

Figure 12: Data presented in Figure 11 are plotted with expanded axes.

We repeated the thermal runaway measurements under identical conditions to assess the variability in the results. Figure 13 shows two sets of data under identical test conditions of heat transfer coefficient and heater power input showing the excellent reproducibility of these measurements. Both the time required for the thermal runaway and the cell surface temperature where the voltage drop occurred are reproduced in the two experiments conducted under identical test conditions.

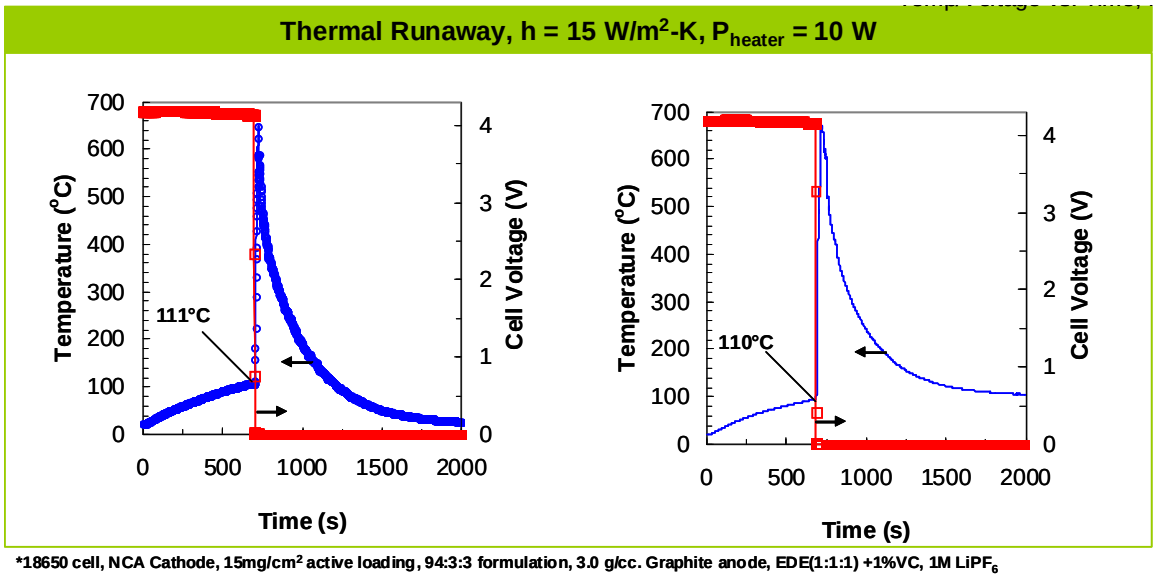

Figure 13: Examples of thermal runaway data for two 18650 cells under identical test conditions. The heater power input was set to ~10 W at time t=0. The air flow rate was set to achieve a surface h of 15 W/m^2-K. The cell incorporated NCA cathode and graphite anode and was based on the baseline design described in Section 4.4.

5.2.1. Variability in the Time/Temperature Curves

Although the time required for thermal runaway and the cell surface temperatures at which a voltage drop occurred were reproduced in our experiments, we did find that the shape of the temperature rise curve was sensitive to the external heat transfer coefficient. Figure 14 shows examples of two distinct shapes for the time/temperature curves labeled 'a' and 'b'. For curves of type a, the cell surface temperature increase is gradual and continuous prior to thermal runaway. In curves of type b, there is an abrupt bump in cell surface temperature when it reaches ~100ºC. A few seconds after this abrupt temperature rise, the rate of temperature rise matches the value before the abrupt rise. Eventually, the cell undergoes thermal runaway when its surface temperature reaches ~156ºC. In general, we observed curves of type b for experiments where the heat transfer coefficient was low and we observed curves of type a where the heat transfer coefficient was relatively high.

The shape of the time/temperature profiles point to important phenomena underlying the thermal runaway processes. As we shall argue in Section 6, the reason for the abrupt rise in cell temperature for curves of type b is likely to be an internal short created by separator melting in the vicinity of the heater. The resistance of the internal short that is created by separator melting is not predictable, and is quite stochastic. If the power dissipated in this short is high, then we would get curves with shape a, whereas if the power dissipated in this short is low, then we would get curves of type b.

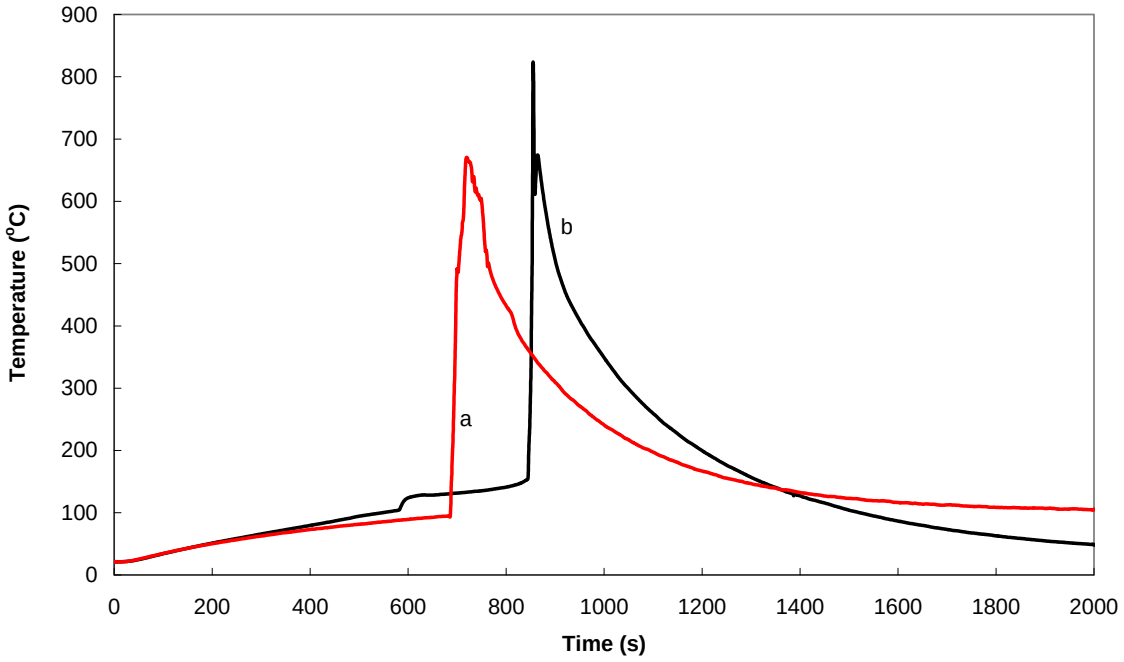

Figure 14: Graph showing two distinctly different shapes for the time/temperature curves (labeled as 'a' or 'b' in the graph) observed in the thermal runaway experiments. The heat transfer coefficient corresponding to curve 'a' was 15 W/m^2-K and that corresponding to curve 'b' was 12 W/m^2-K. The cells used in these experiments incorporated an NCA cathode and graphite anode, and were based on the baseline cell design described in Section 4.4.

5.2.2. Quenching of Thermal Runaway

We also experimentally assessed an earlier prediction[3] based solely on modeling that it would be possible to 'kill' thermal runaway by increasing the rate of heat transfer at the cell surface. Data for such experiments are shown in Figure 15. In this set of experiments, identical NCA cells were tested with heater power of 10 W, and initially identical heat transfer coefficients of 12 W/m^2-K. For the experiment corresponding to curve 'c', the heat transfer coefficient was maintained at 12 W/m^2-K, and the cell experienced thermal runaway when the cell surface temperature reached 156 ºC. The data for temperatures higher than 156 ºC are not shown because the violence of the thermal runaway dislodged the thermocouple. However, visual observation of a red-hot cell, smoke, and flame confirmed that the cell experienced thermal runaway.

In the experiment corresponding to curve 'd', the initial heat transfer coefficient was also 12 W/m^2-K. However, when the cell surface temperature increased to 130ºC, the heat transfer coefficient was increased by a factor of about four to 50 W/m^2-K. As can be seen in the figure, with this increase in the heat transfer coefficient, the cell surface temperature begins to decline and the cell does not experience thermal runaway. This experiment reinforces the point that thermal runaway is a consequence of a prolonged (minimum) period of higher rate of heat generation within the cell than can be removed from the cell. If this rate of heat transfer out from the cell can be controlled, then the progression to thermal runaway can be altered. Future experiments must confirm that thermal runaway can be quenched even when the cell surface

temperature exceeds 156 ºC — the temperature at which thermal runaway occurred in the experiment corresponding to curve c in Figure 15.

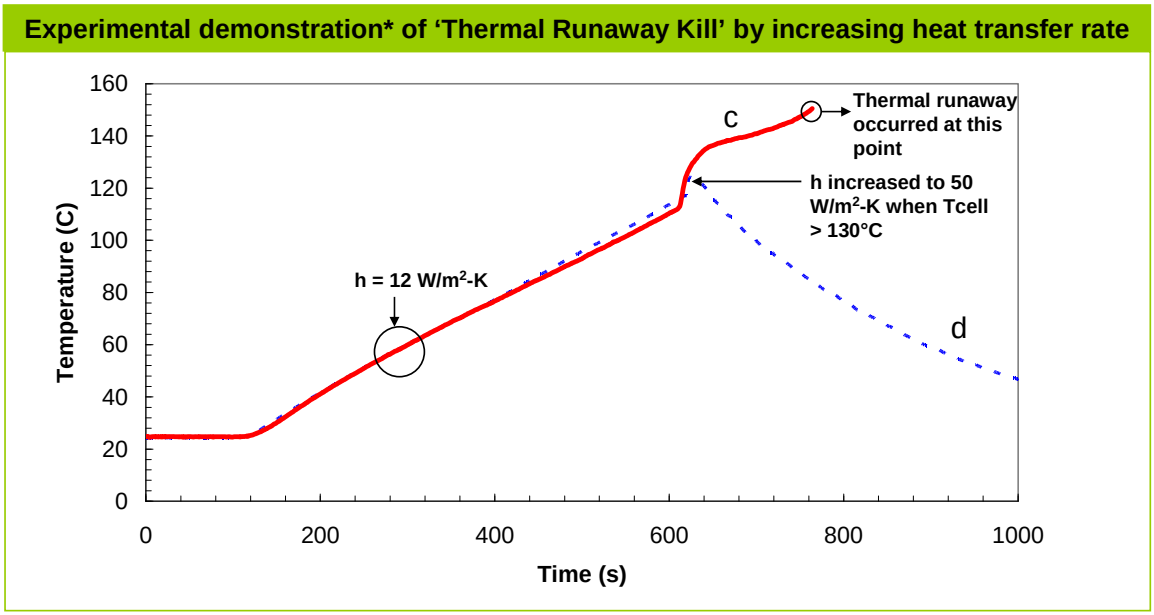

Figure 15: Experimental data for 18650 cells showing that the heat transfer rate can be increased to 'kill' thermal runaway. Tests corresponding to curves 'c' and 'd' in the figure were performed with identical NCA cells designed according to the baseline design described in section 4.4. The test conditions were as follows: heater power = 10 W, heat transfer coefficient initially = 12 W/m^2-K. The heat transfer coefficient was increased to 50 W/m^2-K when the cell surface temperature exceeded 130 ºC in the test corresponding to curve 'd'.

5.2.3. Post-Mortem Analysis of Progression to Thermal Runaway

Quenching of the cell before it experienced thermal runaway provided an opportunity to understand the status of the cell prior to thermal runaway. Accordingly, we performed a tear-down analysis of the cell corresponding to curve d in Figure 15. The cell voltage prior to the tear down analysis was 0.7 V. Figure 16 and Figure 17 show photographs from the tear-down analysis. Figure 16 shows the harvested anode and cathode electrodes. During the tear-down, we observed that a large portion of the separator had shut down. Indeed, a portion of the anode remained fully charged as indicated by its golden color. Furthermore, the remaining portion of the anode was brown in color, again indicating that the anode did not fully discharge at the end of the experiment. These observations, when taken in concert with the creation of the internal short from separator melting, suggest that the separator corresponding to the region of the anode that is golden in color must have shut down before the cell had a chance to discharge through the internal short. The pattern of the charged anode is indicative of the temperature profile at the time the separator shutdown.

Examination of the bare aluminum foil in the core of the jelly roll, that is, the region closest to the heater, clearly shows evidence of the internal short (Figure 17). It appears that the separator between the bare copper foil and bare aluminum foil in the core region melted, allowing the

copper to come into direct contact with the aluminum, and in fact the copper appears visible at one point (circled in figure), possibly indicating high temperature alloying with aluminum has taken place. This result is not surprising given that the separator in the vicinity of the heater would get hot before the rest of the cell would.

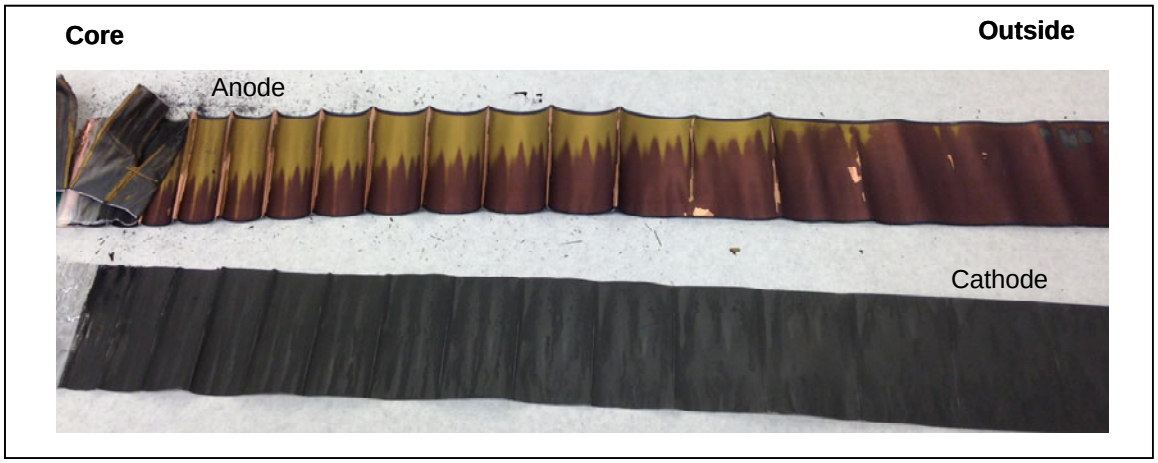

Figure 16: Photographs of the anode and cathode electrodes from tear-down analysis of cell from the experiment corresponding to curve d in Figure 15, following the quenching of the thermal runaway. The part of the electrodes close to the core and the outside of the cell are indicated in the photographs.

Figure 17: Photograph of a part of the cathode from Figure 16 showing a portion of bare aluminum foil that is a part of the core of the cell. The portion of the Al foil circled in red shows a hole in the aluminum foil and the underlying copper foil (from the anode coating) is clearly visible and likely responsible for an internal short circuit induced by melting of the separator between the anode and cathode layers.

The experimental data described in this section were used to calibrate model parameters as summarized in Section 6.

6. Validation of FEA Model for Simulating Thermal Runaway of Li-ion Cells

6.1. Model Overview

We previously developed a thermal model for a lithium-ion cell[4] and this model was updated in this project. The model employs a commercially-available finite element analysis (FEA) code, Abaqus, augmented with custom routines that capture the heat release associated with the presence of short circuits and self-heating of the cell due to exothermal electrode decomposition.

The model simulates transient heat transfer both within the cell and into or out of the cell. The model of the cell can be fully three-dimensional, or two-dimensional, using symmetry as appropriate to lower the computation time required for completing the simulation.

The model was constructed primarily to simulate heat build-up and thermal runaway due to an internal short circuit; however, it can also be used to simulate hotbox tests or cell heat-up during charge and discharge cycles. The model can also be extended to study such things as heat release during nail penetration or cascading in a pack of cells.

An FEA model for a cylindrical lithium-ion cell is pictured in Figure 18. In TIAX's model, the following components of the cell are included:

- jellyroll;
- can;
- cap;
- other components in the cap (PTC and CID);
- insulating plastic disks at each end of jellyroll;
- air pockets inside the cell.

The figure shows both a 3-D depiction of the cell (with one-quarter of the cell cut out) and the 2-D model of the cell, as indicated. The jelly roll is pictured in yellow; open air space is pictured in blue. This cell does not have a mandrel. Note that the individual elements are not shown, due to their small size. This model contains approximately 38,000 elements, with a characteristic element length of approximately 0.13 mm.

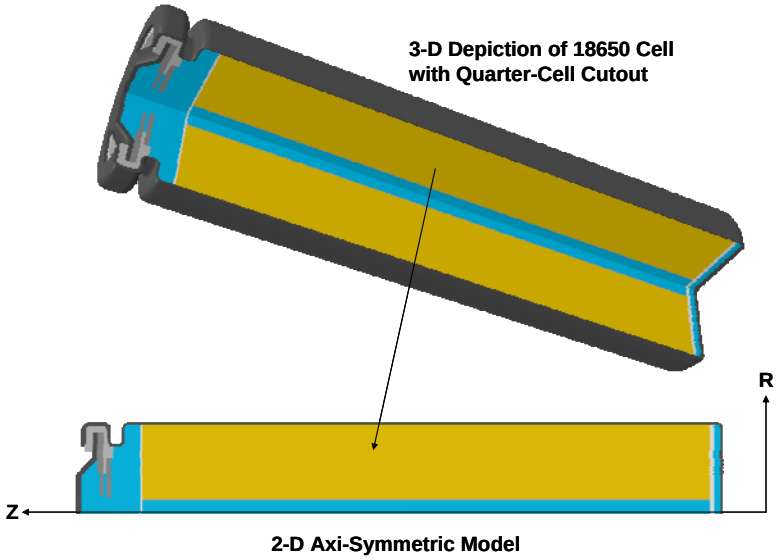

Figure 18: TIAX's FEA model to simulate thermal runaway of an 18650 Li-ion cell.

While efforts have been made to capture the cell geometry accurately, some modifications were made to simplify the cell's geometry and to render it axi-symmetric. For example, the plastic disks that are located below and above the jellyroll have holes in them that were removed.

For each of the components listed above, it is necessary to define three properties:

- conductivity;
- specific heat;
- density.

One key modification was made to the model to shorten the computation time, without sacrificing the accuracy of the predictions: the spiral wound jellyroll is represented as a single, homogenous, cylindrically-shaped component, with material properties derived from the properties of the individual jellyroll constituents (anode, cathode, aluminum current collector, copper current collector, separator, electrolyte). Note that, early-on in the development of TIAX's FEA model for a lithium-ion cell, calculations were made which showed that this simplification has an insignificant effect on model predictions, because the size-scale of the individual electrode layers is very small relative to the size scale of the entire cell.

The properties of the composite jellyroll material were determined based on the following assumptions:

- the spiral-wound geometry of the electrode layers can be represented as a series of concentric rings;
- the density of the composite jellyroll material is defined as the total weight of the jellyroll divided by the total volume of the jellyroll, where it is further assumed that the jellyroll fills the inside of the can completely in the radial direction;

- the specific heat of the jellyroll is defined as the sum of the specific heats of the individual constituents multiplied by their respective weight fractions;
- the conductivity of the composite jellyroll material *in the axial direction* is calculated as the weighted sum of the conductivities of the individual layers multiplied by their respective thicknesses, i.e., as if they are acting in parallel;
- the conductivity of the composite jellyroll material *in the radial direction* is calculated as the inverse weighted sum of the conductivities of the individual layers multiplied by their respective thicknesses, i.e., as if they are acting in series.

Properties for the model were determined based on measurements made on cell components during tear-downs as well as cell heat-up experiments, supplemented with properties taken from the literature. Thermal properties for the composite jellyroll material used in the model are listed in Table 2.

Table 2: Thermal properties for composite jellyroll in an 18650 cell

Property	Model Input Value
Density	2310 kg/m^3
Radial Conductivity	1.1 W/m-K
Axial Conductivity	24.1 W/m-K
Specific Heat	Temperature dependent value increasing from 1100 J/kg-C at 0ºC to 1400 J/kg-C at 500ºC

Transfer of heat through the surface of the cell into the surrounding environment is modeled by specifying a convective film coefficient, a radiative emissivity, and a reference 'sink' temperature. Although it is possible to model heat-up of the surrounding environment, we adopted the realistic assumption that the sink temperature is constant at ambient temperature. Based on comparisons of model predictions with experimental data for cool-down following a runaway, we assume an emissivity of 0.9. The convective heat transfer coefficient is varied to represent the local conditions, which in some of our experiments is characterized by considerable air flow rates.

Heat input from an inserted heater is modeled using the heat generation capability in Abaqus. For a primary internal short, a heat generation rate per unit volume (watts per cubic meter) is specified and applied throughout a single element, which in the axi-symmetric model shown in Figure 18 has a volume of approximately 0.14 mm^3. Simulations performed early-on in the development of the model have demonstrated that, for shorts located near the center of the cell, the thermal behavior of the cell is not significantly different than it would have been if a fully three-dimensional model were used, as the rate of heat conduction in the circumferential direction is quite large, so the heat from a short spreads around the cell quite rapidly. Heat generation from a heater is modeled in the same manner, in which case the heat generation is defined to occur in several elements that take the shape of the heater, rather than in just a single element. We confirmed that both 3-D and 2-D models gave identical results, but the 2-D models

run in a much shorter time and hence this approach was used for most of the 18650 simulations described below in Section 6.3.

Heat generation due to exothermic decomposition reactions is also modeled using the heat generation capabilities of Abaqus. However, unlike heat generation from a short circuit or a heater, which is defined as an input to the model, heat generation due to decomposition reactions must be calculated as part of the numerical solution of the transient heat transfer problem. In order to properly calculate heat generation due to decomposition, we constructed a 'user-added' subroutine for Abaqus that calculates the heat generation rate for a given time interval, and also calculates the incremental extent of reaction within each element of the jelly roll during the time interval and the cumulative extent of reaction over the entire transient. The routine calculates the heat generation rate and tracks the extent of reaction for every reaction that is identified for the cathode and anode. For example, the current model for a TIAX-built 18650 cell assumes that there is 12.9 g of cathode material in the jellyroll, of which 94% is active material. Therefore, if a particular decomposition reaction is found to generate 1500 J/g of active cathode material, the model is set up to generate 1500*12.9*0.94 = 18,200 J of heat for that reaction. The instantaneous rate of heat generation is determined by the local temperature and extent of reaction.

The current model accounts for up to seven reactions, three for the cathode material and four for the anode material. Additional reactions can be modeled, if necessary, through minor modifications to the code. The heat generation rate and cumulative heat generated are tracked throughout the transient and saved as an output file for each reaction. In addition, the distribution of local heat generation rate and cumulative heat generated per unit volume are stored as contour variables and can be visualized in the Abaqus post-processing program and saved.

The subroutine also optionally models heat generation from a secondary short (such as that created from separator melting) and separator shutdown. The secondary short that we have observed in experiments is modeled as heat generation in a single element that is initiated once the temperature in that element reaches a specified value. Based on experimental data (described in Sections 6.2.2 and 6.2.3), we have set the initiation temperature to 166ºC, with the location of the secondary short and the power dissipated in this short defined as an input to the model. Separator shutdown is modeled by identifying elements where the temperature exceeds a separator softening temperature, which is adjustable, but in this work was estimated to be 130ºC. The volume fraction of the jelly roll for which this condition is met is calculated for each time increment. The secondary short power is then reduced based on this fraction. This approach is further described in Section 6.2.2. Note that, to avoid numerical convergence issues, separator shutdown is actually defined to occur gradually and smoothly over the temperature range 120ºC to 140ºC using an error function as described in the next section. This sub-model for separator shut down embodies important assumptions regarding the rate of separator shut down, and must be experimentally verified.

The FEA model for a prismatic cell differs from that of a cylindrical cell only in its geometry and the type of elements that are used in the model. Figure 19 shows the FEA mesh for a representative prismatic PHEV cell, in this case a 33Ah cell that is 21.5 cm high by 13.6 cm wide by 0.77 cm thick. The model uses mostly 3-D 'brick' elements, but also has a few 2-D shell elements to represent the thin tabs. Only one-quarter of the cell is modeled, taking

advantage of two planes of symmetry (left-right and front-back). The same thermal properties listed in Table 2 were used for this cell; with the low conductivity value used for heat conduction through the stack and the high conductivity value applied to the two directions in the plane of the stack. A head space of 4 cm was added above the stack, and filled with air and with several 2.6 cm-wide thin sheets representing tab connections between the various layers of the stack and terminal posts which are added to the top of the cell. A 0.1 mm-thick insulating layer was added all around the stack, and the entire assembly is enclosed in a steel can with a thickness of 0.4 mm on the sides of the cell and 0.6 mm on the top and the bottom of the cell. The overall cell size is 25.6 cm x 13.7 cm x 0.87 cm.

The model uses approximately 55,000 3-D elements plus about 350 shell elements for the tabs. The mesh is more refined near the location of the short. Note that, in order to reduce computation time, this mesh is relatively coarse. Mesh density studies have shown that adding further refinement to the mesh smoothes out high frequency noise that arises when the rates of decomposition become extremely large, but does not significantly alter the results of the analysis.

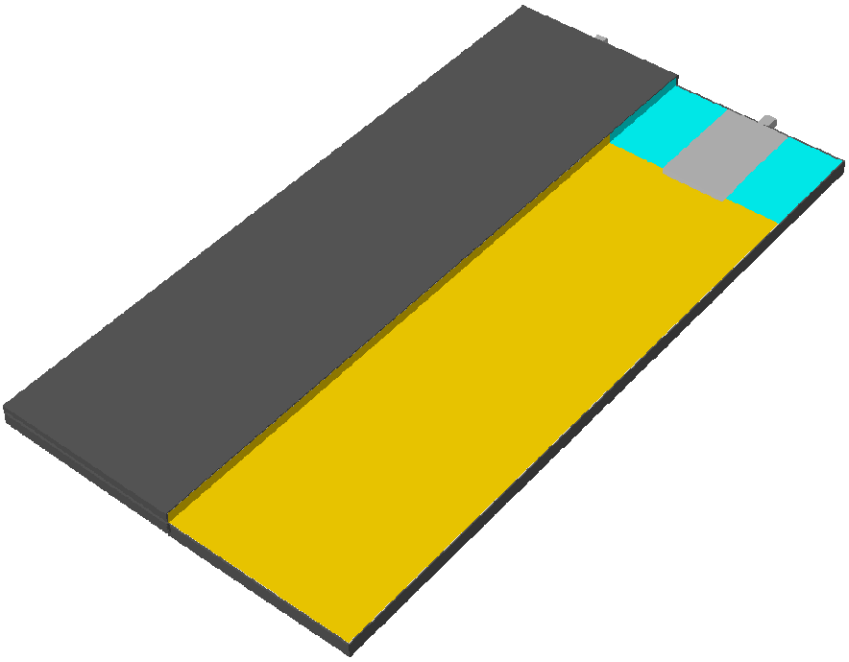

Figure 19: TIAX's FEA model to simulate thermal runaway of a prismatic PHEV cell (with one quarter of the cell cut out. Taking advantage of symmetry, only one quarter of the cell need be modeled. The electrode stack is pictured in yellow; open air space is pictured in blue. This model also includes representations of tabs (shown in grey) and terminals. The model uses approximately 55,000 3-D elements plus about 350 shell elements for the tabs.

6.2. Estimation of Model Parameters

In this sub-section, we summarize the generation of key input parameters for the model.

6.2.1. Sub-Model for Heat Release Kinetics

Heat release from the anode and cathode decomposition reactions are critical inputs for thermal runaway simulations of Li-ion cells. As described in the earlier sections, the anode and cathode materials used in a typical Li-ion cell can undergo exothermic reactions at elevated temperatures. Given the importance of obtaining a good mathematical representation of the kinetics of heat release from the anode and cathode reactions, we strongly recommend a first-principles approach to deriving suitable kinetics expressions such that the heat release kinetics can be estimated under a wide range of conditions. Such an approach was outside the scope of the present work, and we employed reasonable kinetic expressions, whose parameters were estimated by fitting experimentally obtained heat release data.

Here we summarize our approach to developing suitable kinetic sub-models to represent the heat release from the anode and cathode decomposition kinetics. We employed Differential Scanning Calorimetry (DSC) measurements of charged anode and cathode materials to obtain data for the heat release kinetics. At TIAX, we have developed methods to obtain reproducible DSC data on Li-ion battery materials. We typically run at least three replicates for every sample characterization. Charged materials are harvested from half-cells, and placed in contact with electrolyte prior to the test. Figure 20 shows the DSC data for the anode and cathode materials employed in the 18650 cells. Figure 20 also shows the kinetic sub-model fits obtained for the anode and cathode decomposition reactions.

The anode decomposition reactions initiate at a relatively low temperature of 150 ºC, but the rate of reaction is low. The rate becomes significant once the temperature exceeds 200 ºC. In other measurements, we found that the onset for decomposition reactions depends on the type of anode materials employed. For some anode materials, the decomposition reactions can begin at temperatures as low as 80 ºC with reasonably high rates (~1 W/g). Exothermic heat release from ~80-120ºC is the initial degradation process and is largely attributed to decomposition of the solid electrolyte interface (SEI) at the anode surface, and reaction of freshly exposed carbon surface with the electrolyte. Exothermic heat release between ~150-300°C is attributed to both reaction of salt with solvent as well as reduction of the electrolyte due to bulk decomposition of the anode.

To obtain a fit to these anode kinetic data, we used a modified Avrami-Erofeev kinetics model. As shown in Figure 20, the kinetic sub-model is able to provide a good fit to the experimental data. However, we note that the kinetic rate expression is at best a fit to the data and additional work is needed to derive a model for heat release based on a ‘first principles’ approach.

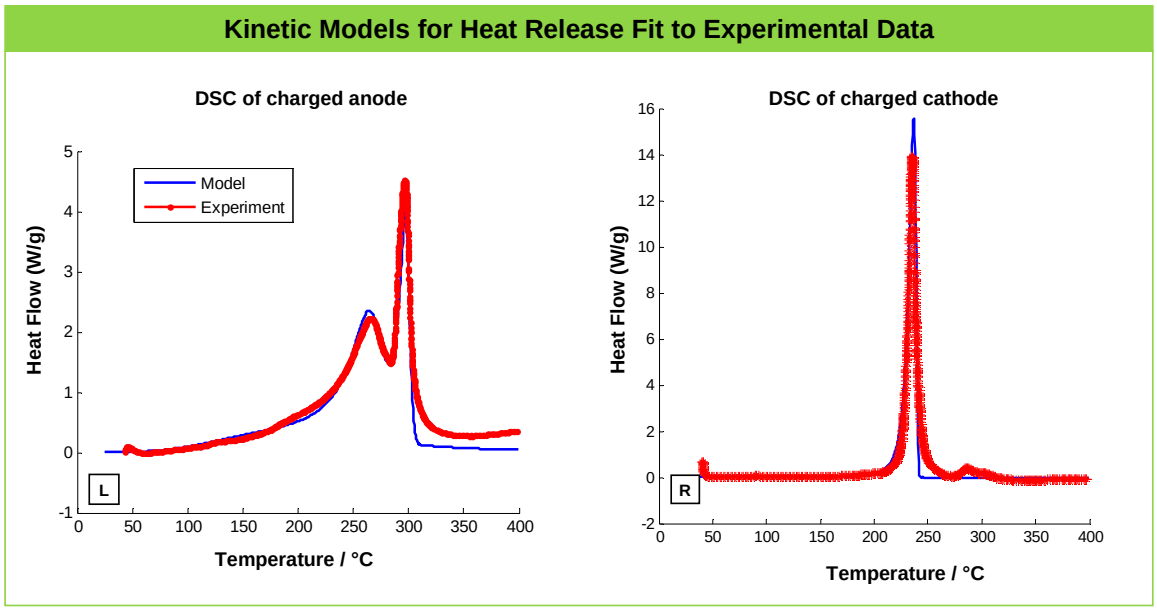

Figure 20: Figures comparing the differential scanning calorimetry (DSC) data for charged anode and cathode materials with model representations of the heat release kinetics. For these measurements, half-cells were used for charging the graphite anode (to 0.1 V vs. Li metal) and NCA cathode (4.3 V vs. Li metal). Subsequently, the charged electrodes were harvested from the coin cells and placed in a DSC pan in contact with the electrolyte used in the 18650 cells for the heat release measurements. The scan rate in the DSC measurements was 5 ºC/min. The kinetic sub-models that gave these fits were based on modified Erofeev-Avrami models. The materials used in these experiments were the same ones used in the 18650 NCA cells.

6.3. Calibration of Model Parameters

We calibrated the model parameters by using the experimental data from Section 5. A comparison between the experimental data and the model fit is shown in Figure 21. The only adjustable parameter was the power dissipated through the secondary short that is created when the separator temperature in the core exceeds 166ºC. The secondary short power that best fits the experimental data was 100 W, as is described further below. All the other input parameters were either separately measured (such as the kinetic models for heat release, electrode and cell dimensions, thermal properties of the cell components, etc.) or taken from the literature (e.g., specific heat of the steel, copper and aluminum).

As can be seen, the fit to the experimental data is good. The model is able to predict not only the initial rate of rise of the cell surface temperature due to internal heating by the heater, but also the temperature at which the thermal runaway occurs. Moreover, the rate of temperature increase during thermal runaway closely matches the experimentally observed rates. There is some discrepancy between the maximum temperature experimentally recorded and that predicted from the simulations. This discrepancy can be attributed to the fact that significant amounts of active material and electrolyte are ejected from the cell during thermal runaway and hence would not be contributing to the heat release during the thermal runaway. In addition, vent opening and ejection of cell components would have a quenching effect. These phenomena are not captured in our model, and hence it is not surprising that the model predicts a higher temperature than is actually measured.

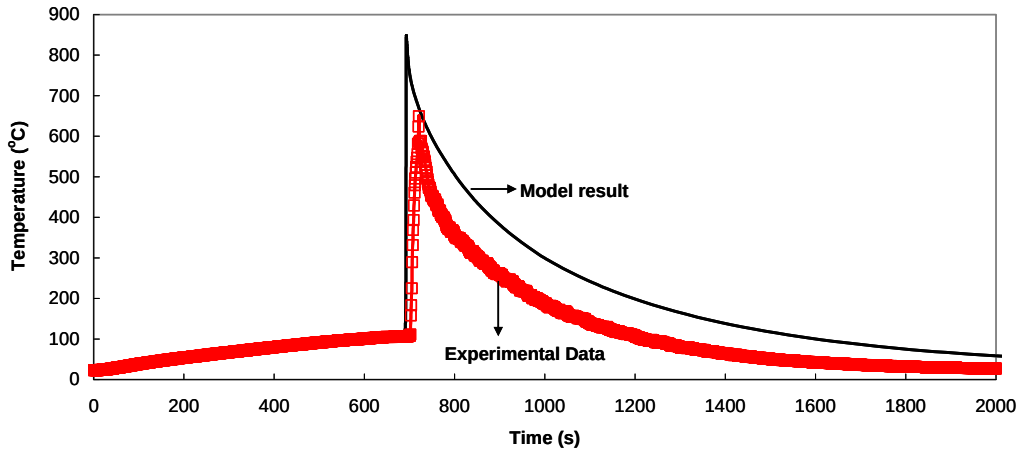

Figure 21: Comparison of the experimentally measured surface temperature for a thermal runaway experiment and the model fit to the experimental data. The only adjustable parameter for the model was the initial power delivered to the secondary short, and is described in the text. The conditions were: heater power of 10 W, and a heat transfer coefficient of 15 W/m^2-K.

It is instructive to examine the details of the simulation results to understand the progression towards thermal runaway. The model predicts that thermal runaway occurs when the cell surface temperature reaches 110ºC, which is a temperature lower than that needed to stimulate significant heat release from the anode or cathode decomposition reactions. However, examining the temperature profiles provides significant insight into the progression to thermal runaway.

Figure 22 shows the temperature distribution within the cell at three different points in time (103 s, 344 s, and 594 s) before thermal runaway occurs. As can be seen from the figures, even though the heater temperature can be as high as 500ºC, the bulk of the cell is at a much lower and nearly uniform temperature indicating that, under these conditions, the rate of heat transfer within the cell is higher than the rate of heat removal at the cell surface, resulting in nearly uniform temperature within the cell. It is only the region that is in the immediate vicinity of the heater that is at a slightly higher temperature.

Figure 23 shows the temperature profile in the cell just before thermal runaway occurs, i.e., at ~675s. As observed experimentally, the cell surface temperature is ~110ºC at this point in time. Also noteworthy is that, at this point in time, the temperature of the cell in the vicinity of the heater is > 166ºC, the temperature at which the separator melts (per the data in the previous section). Note that the regions of the cell that are at temperatures in excess of 170ºC have been shaded gray (essentially an expanded scale for temperature). Therefore, it is not surprising that the secondary internal short occurs when the cell surface temperature is ~110ºC under these conditions, in accordance with the experimental data described in Section 5.2.

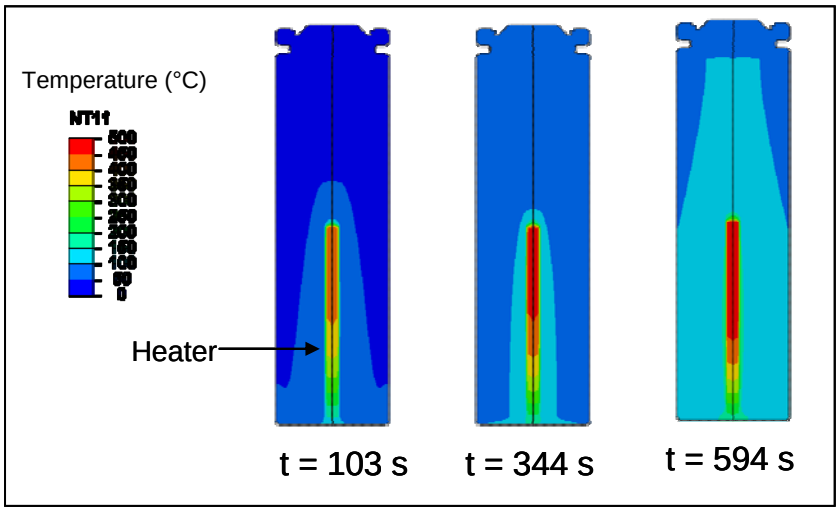

Figure 22: Simulation results of temperature distribution in the cell corresponding to the modeling results shown in Figure 21 for three different points in time.

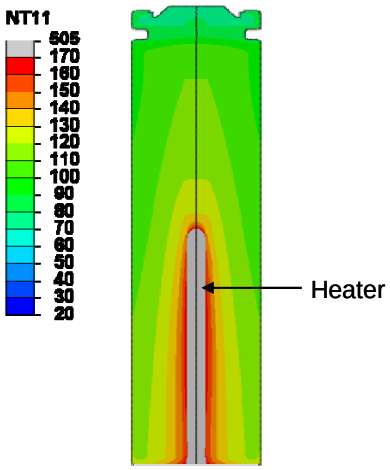

Figure 23: Cell temperature profile at 675 s from the simulation results shown in Figure 21, i.e., just before thermal runaway occurs in the cell. For this plot, the areas of the cell that are above 170ºC have been shaded gray.

Also, the contours of temperature seen in Figure 23 match the charged anode pattern seen in the previous section for the post mortem of a cell that was quenched after the hard short occurred. Essentially, the temperature contours suggest that a greater fraction of the separator will be shut down closer to the heater than farther away from the heater. This can be visualized better in Figure 24, where the fraction of the cell that is at a temperature less than 130ºC is colored gray.

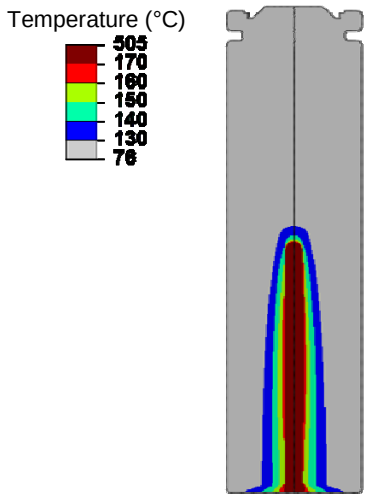

Figure 24: Same conditions as for Figure 23, except that the region of the cell that is at temperatures less than 130ºC has been colored gray.

Figure 25 shows the fraction of the separator that has shut down as a function of time. The separator shutdown is initiated around 300 s. At the point of thermal runaway (675 s), only about 10% of the total separator is shutdown, suggesting that a major fraction of the jelly roll is available to feed the secondary short that is created when the separator melts at 675 s.

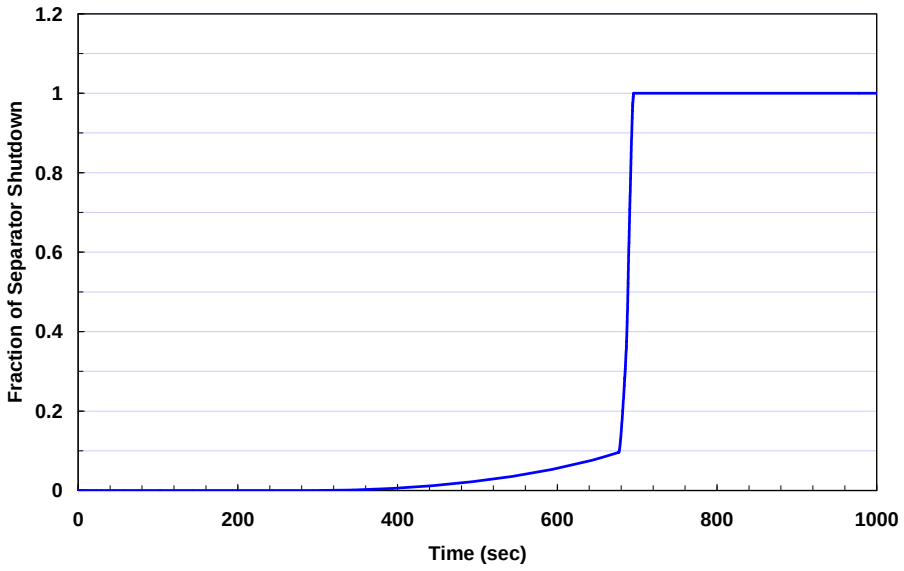

Figure 25: Fraction of separator that is shutdown as a function of the time corresponding to the simulation data in Figure 21. Only ~10 % of the separator is shut down by the time thermal runaway occurs.

Figure 26 shows the cumulative heat release (integrated over the volume of the jelly roll) from the different heat sources in the cell corresponding to the simulation results in Figure 21. The inset shows the cumulative heat released with an expanded x-axis around 675 s. The constant power deposited in the heater is the only significant source of heat in the cell prior to thermal runaway. Prior to runaway, the heat release from the anode decomposition reactions is about

three orders of magnitude higher than that from the cathode decomposition reactions. This ratio is not surprising given that the anode decomposition reactions have a lower onset temperature than those for the cathode. It is noteworthy that it is the separator melting and activation of a secondary short that has led to the thermal runaway. The cathode decomposition by itself was not sufficient to cause thermal runaway under these conditions.

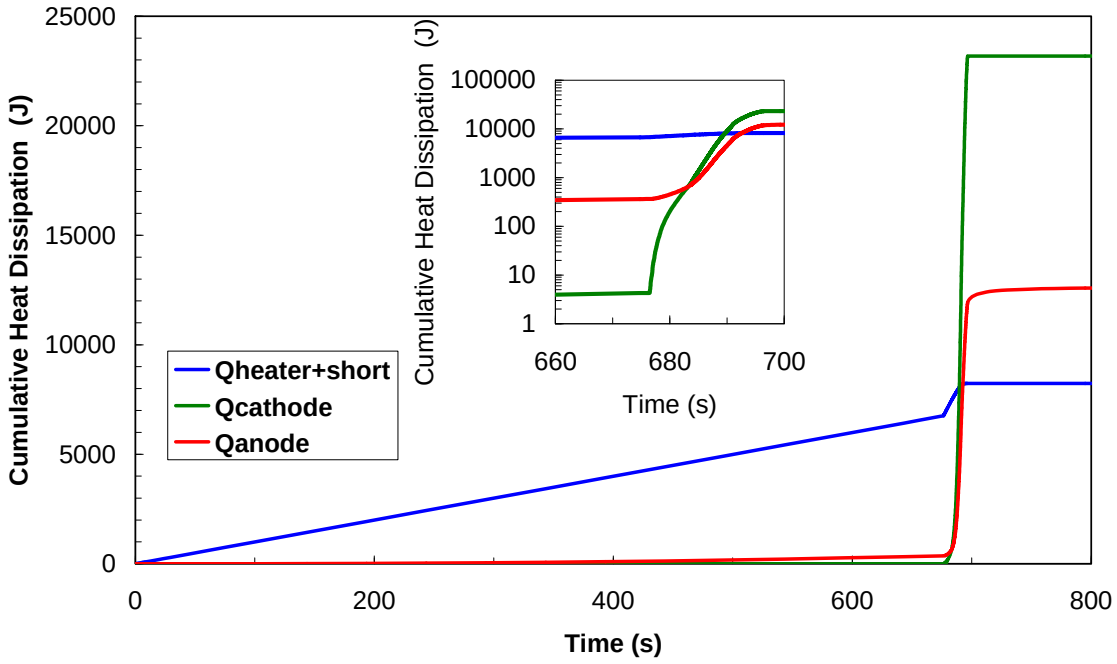

Figure 26: Cumulative heat release from the different heat sources in the model corresponding to the simulation data in Figure 21.

In summary, the model calibration (with only one adjustable parameter) has shown the following:

- The onset temperature for thermal runaway from the simulations matches closely with the experimental data.
- The rate of temperature rise during thermal runaway from the model matches well with the experimental data.
- The model appears to over-estimate the peak temperature. This discrepancy is most likely due to the ejection of active materials during thermal runaway, thereby removing energetic reactants from the reaction zone inside the cell and limiting the heat that could be generated in the experiment, and the quenching effect of cell venting. These phenomena are not accounted for in the simulations.
- Simulation results explain why the secondary short occurred in the cell when the surface temperature reached 110ºC. Simulation results show that the separator in the vicinity of the heater reaches 166ºC when the surface temperature reaches 110ºC. Under these conditions, the separator in the vicinity of the heater must have melted, causing the secondary short. We determined a value of 100 W for the secondary short power. However, power values higher

than 100 W or slightly lower than 100 W would have yielded the same result. At the moment, there is no theoretical basis to estimate the exact value of this secondary short power and it may well be different based on different cell designs, electrode formulations and materials employed. Separate work being done at TIAX suggests that the electrodes used in a typical Li-ion cell are capable of short-term power dissipation well over a kilo-watt in an 18650 cell, suggesting that much higher values for the secondary power can result under suitable conditions.

- Prior to thermal runway, the heat release from the anode and cathode decomposition reactions was not significant. The primary reason for thermal runaway, therefore, is the heat deposited by the heater as well as the power dissipated in the secondary short.
- The extent of separator shutdown prior to thermal runaway is only about 10%, suggesting the majority of the cell is available to supply power to the secondary internal short.

6.4. Effect of Reduced Secondary Short Power

As described in Section 5.2, we observed a different temperature/time curve than the one illustrated in Figure 21. Using the secondary short power as a variable, we attempted to fit the experimental data, as shown in Figure 27. Assuming a low impedance for the secondary short, such that most of the power was delivered in the jelly roll when the secondary short formed, we were able to get a good match to the abrupt rise in cell surface temperature at ~577 s. Essentially, the secondary short occurred at 577 s, and we assumed that most of the power in the secondary short was delivered in the jelly roll. The model also fits the rate of temperature rise until about 800s.

The reasons for the poor fit to the time of thermal runaway or the temperature at which thermal runaway occurs are not clear at the moment. One possibility is that there are additional secondary shorts created within the cell at around 800 s that cause localized heating and hence thermal runaway. Another possibility is that the kinetics sub-model for the anode and cathode decomposition kinetics we are using have to be refined to predict the rate of heat release especially at high temperatures.

Nevertheless, examining the modeling results provides clues regarding the reasons that the thermal runaway did not occur immediately following the secondary short. Figure 28 shows the fraction of the separator that has shutdown corresponding to the model results in Figure 27. As can be seen here, only 10% of the separator has shut down prior to the occurrence of the secondary short. However, the distributed heating of the cell allows most of the cell to rapidly reach 130ºC, and 90% of the separator is shut down within 50 s of the occurrence of the secondary short. Under these conditions, power dissipation through the secondary short cannot be sustained. The increasing fraction of separator shutdown with time implies that the energy dissipated in the jelly roll decreases, thereby the rate of temperature rise decreases.

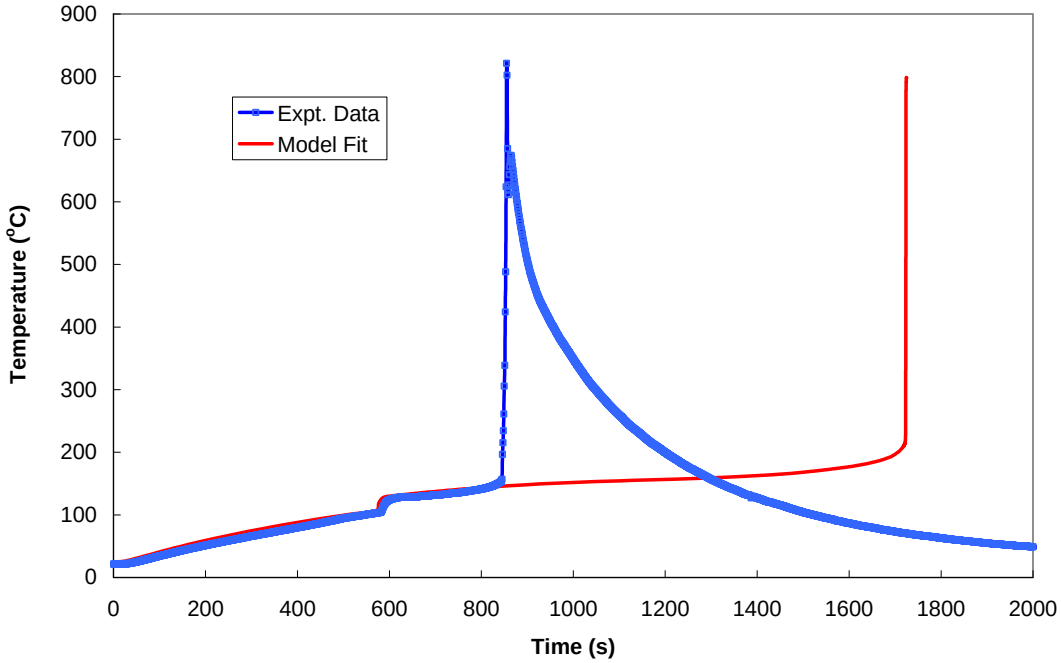

Figure 27: Comparison of the experimentally measured surface temperature for a thermal runaway experiment and the model fit to the experimental data. The only adjustable parameter for the model was the initial power delivered to the hard short, and is described in the text. The conditions were: heater power of 10 W, and a heat transfer coefficient of 12 W/m^2-K.

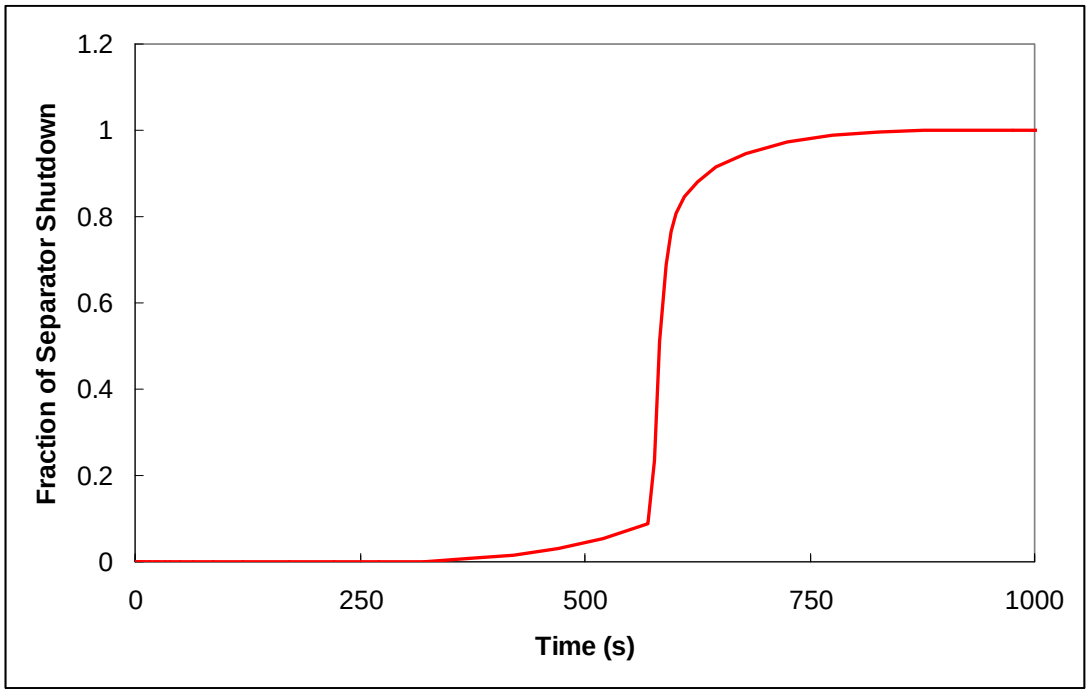

Figure 28: Fraction of separator that shutdown as a function of time.

6.5. Quenching of Thermal Runaway

As described in the previous section, we experimentally demonstrated that thermal runaway could be eliminated by opportunistically increasing the rate of heat transfer. Here, we show simulation results corresponding to this case. Figure 29 shows a comparison of the simulated cell temperature profile with experimental data. The shape of the time/temperature curves for the simulation and experiment are similar. The simulation results show quenching of thermal runaway because of the increased heat transfer coefficient. However, there is a slight discrepancy in the time needed for the hard internal short and the abrupt rise in cell temperature. This discrepancy could occur because the power in the heater was not exactly 10 W in the experiment, but slightly lower. Regardless, the model is able to adequately capture the trends.

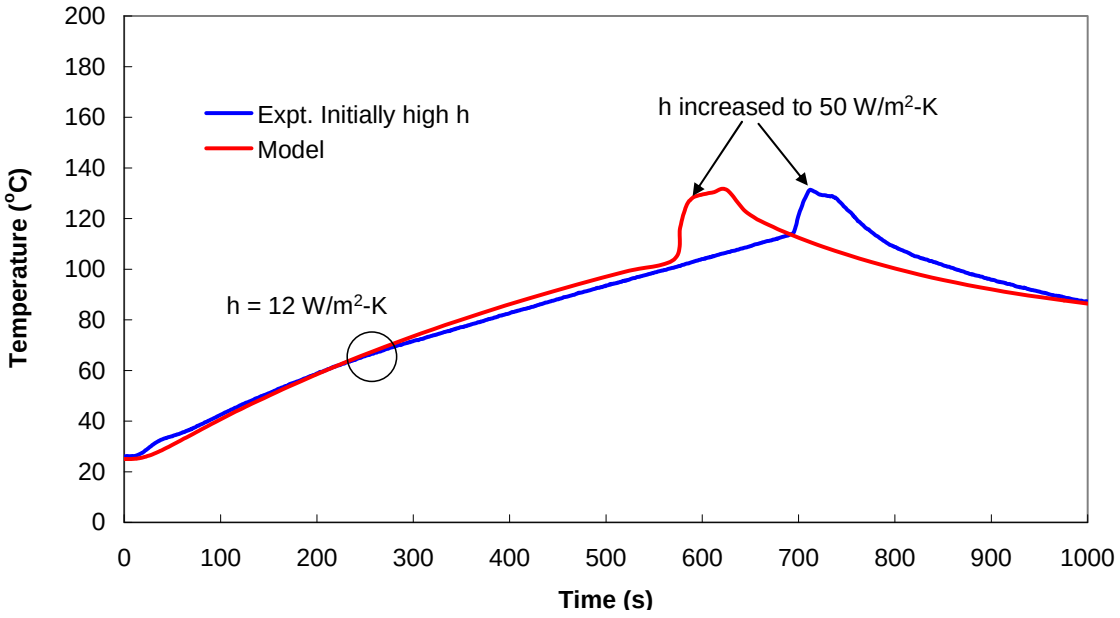

Figure 29: Comparison of experimental and simulated temperature profiles for the thermal runaway quench experiment. In these experiments and the corresponding simulation, initially low h was increased by a factor of ~ 4 when the surface temperature exceeded 130ºC. The heater power was 10 W.

The results in this section show that the FEA model, with only the power delivered in the secondary short as an adjustable parameter, is able to capture the experimentally measured data for thermal runway of Li-ion cell fabricated at the TIAX facility. In the next section, we will use this model with calibrated parameters to assess the impact of cell design variables and environmental conditions on thermal runaway of prismatic PHEV-size cells.

7. Simulation of PHEV-Size Cells

Previous section of this report summarized validation of the FEA thermal model through comparison of model predictions for an 18650 cell with well-characterized thermal runaway experiments. This section summarizes application of the model to full-size PHEV-size cells, with the overall objectives of understanding the factors that control the thermal runaway of PHEV cells and identifying strategies to reduce the probability of thermal runaway. Accordingly, simulations of internal short-induced thermal runaway in 33 Ah PHEV cells were aimed at:

- understanding differences between PHEV cell and 18650 cell behavior;
- understanding the effect of various cell design parameters and environmental conditions on cell behavior and, in particular, the conditions for thermal runaway.

It is important to clarify the terminology used in the following discussion with respect to the internal short circuit power dissipation:

- Threshold power is the minimum power (in a short) that results in a thermal runaway. It corresponds to the condition at which heat generated in an internal short or shorts is exactly counter-balanced by the cell's ability to shed that heat. The latter is a function of cell design and also the prevailing heat transfer conditions at the cell surface. A higher threshold power means that stronger internal shorts could exist without a cell progressing to thermal runaway. Increasing the rate of heat transfer at the cell surface increases the threshold power. The threshold power is therefore a useful metric to understand the relative influence of cell design and environmental conditions on the propensity for thermal runaway.
- Primary short circuit power refers to the heat dissipation from the initiating internal short circuit located at the center of the cell. The power cited for the threshold power in the following discussion refers to the primary short power. The primary short power is varied in the simulations in order to identify the threshold conditions for thermal runaway.
- Secondary short circuit power refers to heat dissipation in a secondary internal short circuit that forms when the separator melts allowing for contact between the anode and the cathode. The secondary short power was fixed at 100 W for the baseline case, but the sensitivity of the simulation results to this assumption was evaluated.

7.1. Baseline Calculations

A set of baseline calculations was first performed to determine the threshold value for the primary short power for thermal runaway for a short circuit located at the center of a PHEV cell. This baseline set of calculations was performed for the following conditions:

- A prismatic cell geometry with dimensions of 21.5 cm height x 13.6 cm width x 0.77 cm depth
- NCA cathode material;
- graphite anode material;

- a primary internal short circuit power dissipation that is varied in the simulations, and this primary internal short is assumed to occur at the geometric center of the cell;
- a secondary short power dissipation in the vicinity of the primary short circuit. As with the 18650 simulations, we assume that a secondary short will occur in the cell when the separator temperature exceeds 166ºC. We use the baseline value of 100 W for the secondary short power, which was used for fitting the 18650 experimental data. We recognize that the power capability of larger cells would be significant relative to 18650 cells, and the sensitivity to the secondary short power is treated in the section on sensitivity analysis. This secondary short is assumed to occur 0.5 mm away from the primary short circuit;
- separator shutdown, occurring at a mean temperature of 130ºC;
- gradual reduction of secondary short power based on the percentage of cell volume in which the separator has shut down;
- a surface heat transfer rate of 12 W/m^2-K, which corresponds to a cell surrounded by quiescent air at ambient temperature. We assume that the air temperature is constant.

A series of analyses was then performed to evaluate the effect of certain key cell parameters on the behavior of the PHEV cell and, in particular, its tendency to runaway, and to establish differences between these tendencies with those of 18650 cells. Finally, a series of analyses was run to determine the effects of intervention to quench a impending runaway.

7.2. Results: Baseline Model

The results from the baseline model are summarized here. We found that the threshold power for the PHEV cell was higher than that for the 18650 cell. In comparison to the smaller 18650 cell, it generally takes more energy to heat up a PHEV cell, due to its greater heat capacity. In addition, there is a greater volume of material around a centrally-located short circuit to act as a sink for the heat generated by the short. Finally, the surface-to-volume ratio for a PHEV cell shaped as modeled is higher than that of an 18650 cell, plus, the relative in-plane vs. through-thickness thermal conductivities of the cell are more conducive to the dissipated heat reaching the surface (i.e., the thickness of the cell is smallest in the orientation where the conductivity is smallest, so transfer of heat to the surface of the cell is not as limited by poor thermal conductivity).

For the baseline model, FEA calculations indicate that the threshold power for thermal runaway is approximately 22 W. Because the model now captures the phenomenon of triggering a higher-power secondary short by heating regions close to the original short, we find that there are three modes of behavior that are observed for the baseline conditions, depending on the primary internal short power, as illustrated in the next several figures:

Primary short power < 18 W: If the primary short power is low enough, then the region near the short never reaches 166ºC, so the 100 W secondary short is never triggered and the cell has no chance of experiencing thermal runaway at a heat transfer coefficient of 12 W/m^2-K. For example, if the primary short power is 15 W, the temperature 0.5 mm away from the short reaches only about 139ºC. If this primary short power is increased to 18 W, the temperature in the vicinity of the secondary short reaches 162ºC. For these cases, a steady-state is reached in which the heat exiting the cell through its surfaces is equal to that being generated by the short, and the temperature doesn't change until the electrochemical energy in the cell is exhausted.

Figure 30 shows the history of temperature vs. time for three points in the cell for the 18 W case: near the short, on the surface of the cell at the center of the large side (closest point to the short), and at the surface of the cell at the center of the thin side of the cell. While the temperature near the short grows to 162ºC, the temperature at the surface of the cell reaches only 65ºC nearest the short and 49ºC at the center of the side of the can. These conclusions would change if better separator melt measurements show that the secondary shorts can occur at temperatures lower than 166 ºC.

Primary short power of 20 W: If the primary short power is increased to 20 W, the region near the short does reach 166ºC (after about 13 minutes), as is shown in Figure 31, and the 100 W secondary short is triggered. The temperature in the vicinity of the secondary short increases dramatically, to over 900ºC; however, this heat is dissipated quickly by the surrounding cell material, and the temperature at the surface of the cell rises much more slowly. Figure 32 shows the time-histories of the heat generation rates due to the internal short (both primary and secondary) and due to decomposition of the anode and cathode materials, as well as the sum of these three components. As the cell heats up, the temperature gradually increases above 130ºC throughout much of the cell, causing separator shutdown. This progression causes the secondary short power to decrease significantly — from 100 W at 13 minutes to only about 20 W after about 30 minutes (i.e., the total short power decreases from 120 W to about 40 W). During this same time period, there is a significant release of heat from the anode and cathode decomposition reactions, but not enough to push the cell into thermal runaway. Once the short power decreases, the temperature throughout the cell begins to gradually decrease to a steady state in which about 40 W of power is being generated by the hard short, and 40 W of power is leaving the surface of the cell. Heat generation from the decomposition reactions gradually decreases as those regions of the cell that are hot enough to cause significant decomposition are exhausted. Interestingly, the steady-state temperature in the vicinity of the short stays at about 360ºC. The simulation was ended after 100 minutes, but it should be noted that eventually the supply of power to the shorts would be electrochemically exhausted, and the cell would cool down to ambient after about 180 minutes.

Primary short power of 22 W: If the primary short power is increased just a little bit, to 22 W, the cell runs away, as noted above. Figure 33 and Figure 34 show the temperature and heat generation rate time-histories for this case. The curves are similar to those for the 20 W case for the first 20 minutes or so. However, because we have introduced a little more heat into the cell during this time period, the cell heats up just enough that the decomposition reactions take over, releasing heat at a rate that cannot be shed from the cell surface, for the assumed heat transfer conditions, and the heat generation rate increases to very large values after about 26 minutes or so.

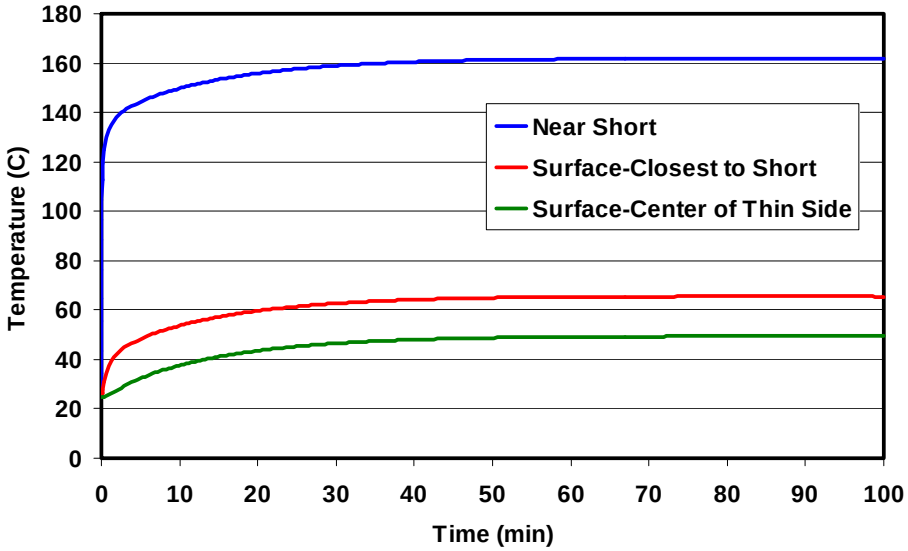

Figure 30: History of temperature versus time for three points in the cell: (1) near the short; (2) on the surface of the cell at the center of the large side (closest point to the short); and (3) at the surface of the cell at the center of its small side, for a primary short power of 18 W.

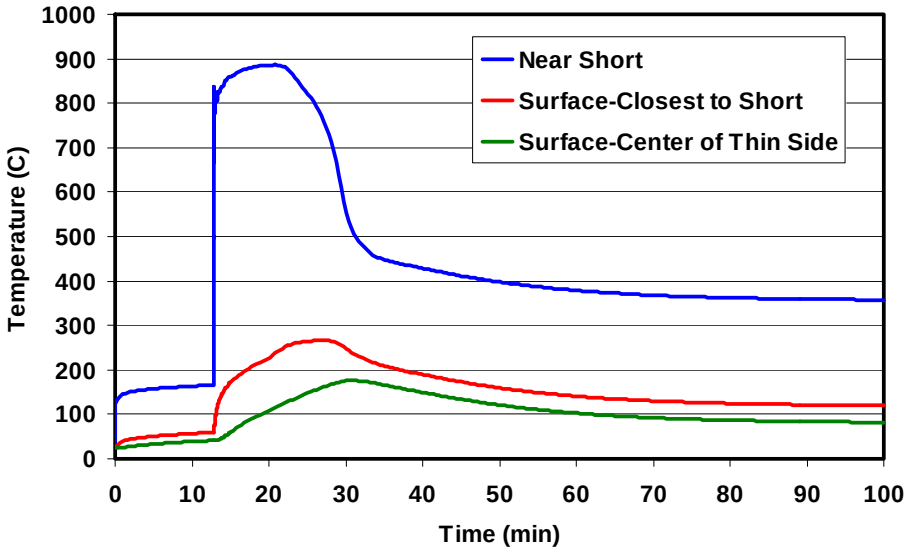

Figure 31: History of temperature versus time for three points in the cell: (1) near the short; (2) on the surface of the cell at the center of the large side (closest point to the short); and (3) at the surface of the cell at the center of its small side, for a primary short power of 20 W.

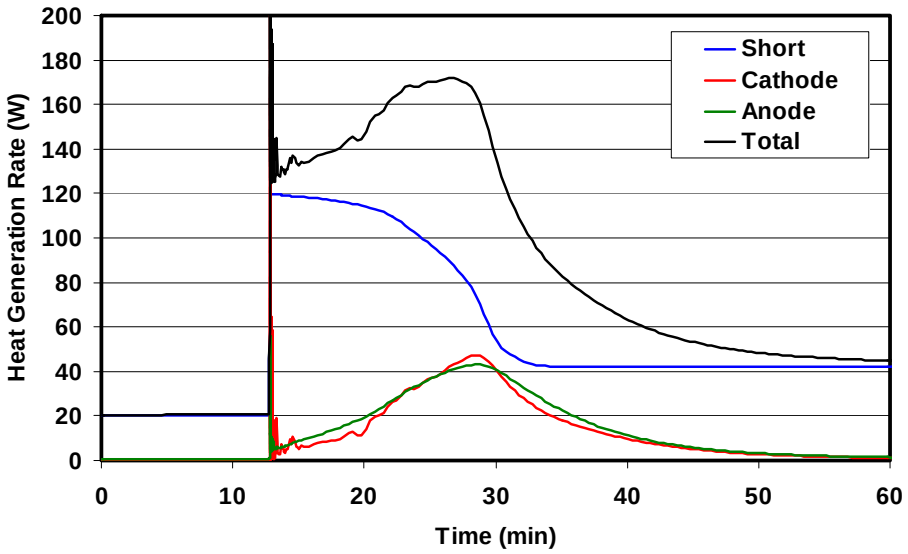

Figure 32: Heat dissipation rate versus time for: the short (combined values of the primary and secondary shorts); decomposition of the cathode; decomposition of the anode, and the sum of all three components for a primary short power of 20 W.

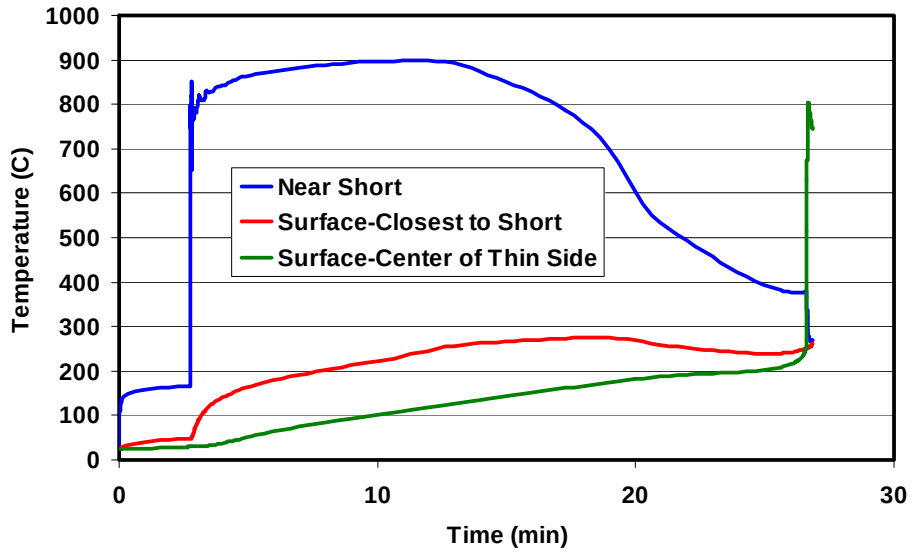

Figure 33: History of temperature versus time for three points in the cell: (1) near the short; (2) on the surface of the cell at the center of the large side (closest point to the short); and (3) at the surface of the cell at the center of its small side, for a primary short power of 22 W.

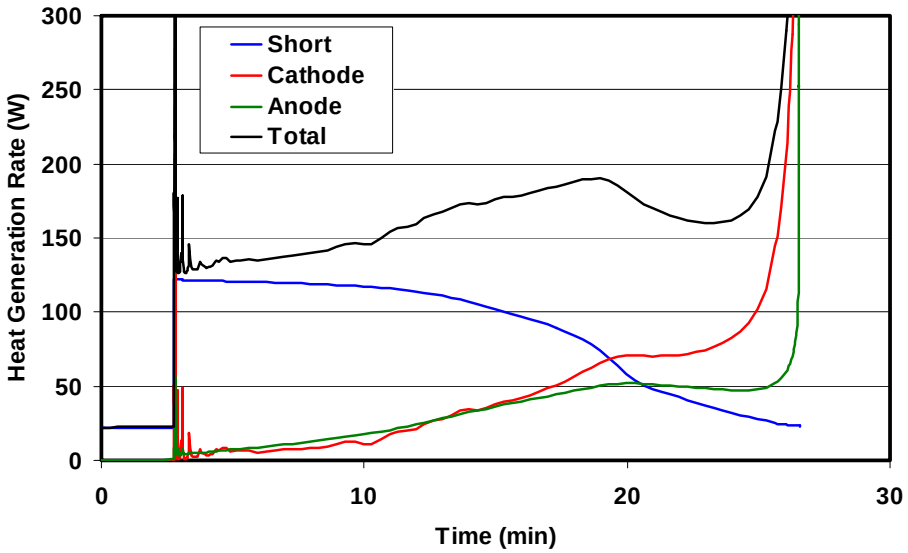

Figure 34: Heat dissipation rate versus time for: the short (combined values of the primary and secondary short power); decomposition of the cathode; decomposition of the anode; and the sum of all three components for a primary short power of 22 W.

For the threshold power case of 22W, Figure 35 illustrates the temperature contours at the onset and during propagation of the thermal runaway. After 22 minutes (left side of Figure 35), the temperature near the short is about 500ºC, and there are nearly circular contours of temperature around this hot spot that are interrupted as the surface of the cell is reached. At 27 minutes (right side of Figure 35) the areas of intense heating are propagating towards the respective sides of the cell, where there is less of a temperature sink due to the lower heat transfer rate through the surface. The center of the cell is actually cooling, as indicated in Figure 33. At this point, the rest of the cell heats up very quickly.

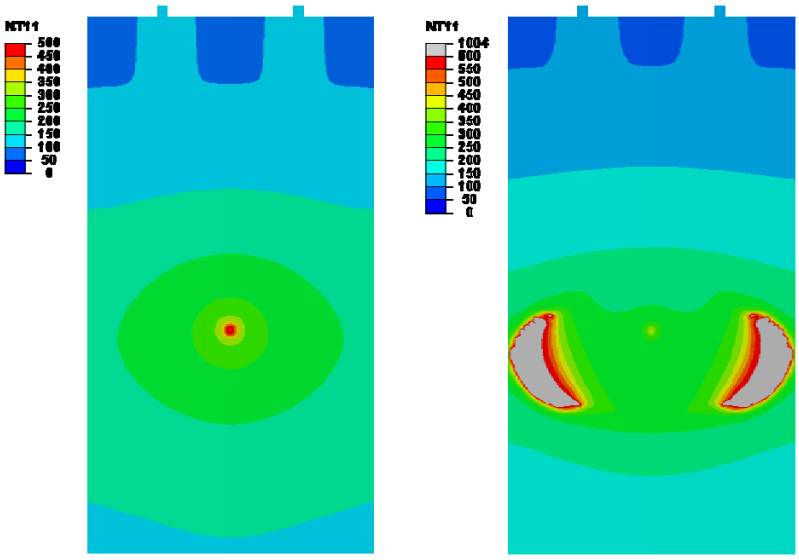

Figure 35: Baseline PHEV model: 22 W short power — temperature contours (slice through center of cell) at 22 minutes (left) and 29 minutes (right) illustrating onset and propagation of runaway.

7.3. Results: Sensitivity to Baseline Model Assumptions

In addition to the baseline model described above, we conducted a series of analyses for several variations on the baseline model, i.e., changes that do not represent modifications to the design of the cell or the surrounding environment but primarily to the power dissipated in the secondary short, including the following cases:

- *No secondary short:* In this case, we assume that the separator does not melt and hence there is no secondary short even when the local temperature exceeds 166ºC;
- *Low power dissipation in the secondary short but high power dissipation in the bulk of the cell:* In this case we assume that the resistance of the secondary short is so low that most of the power from the self-discharge of the cell is dissipated in the cell, i.e., power of 100 W distributed throughout the stack. This situation converges to the case of cell discharge through an external low-impedance short;
- *Higher power dissipation in the secondary short:* To simulate this condition, we assumed that the secondary short power is increased to 200 W from the baseline case of 100 W. Note that recent data from TIAX tests in a separate project have indicated that extremely high powers are possible in secondary short situations. Consequently, we also evaluated the case of 1000 W dissipation in the secondary short.

7.3.1. No Secondary Power Dissipation

If a secondary short is not activated by the initial short, the threshold power for runaway of the primary short increases significantly — to about 75 W. Time-histories of temperature at the three locations identified above are indicated in Figure 36. Despite the high power, the runaway does not occur until after approximately 73 minutes, with the surface temperature closest to the short reaching about 275ºC, and the surface temperature on the side of the cell reaching about 200ºC. Of course, if the external heat transfer coefficient were lower than 12 W/m^2-K, then the threshold power would be lower.

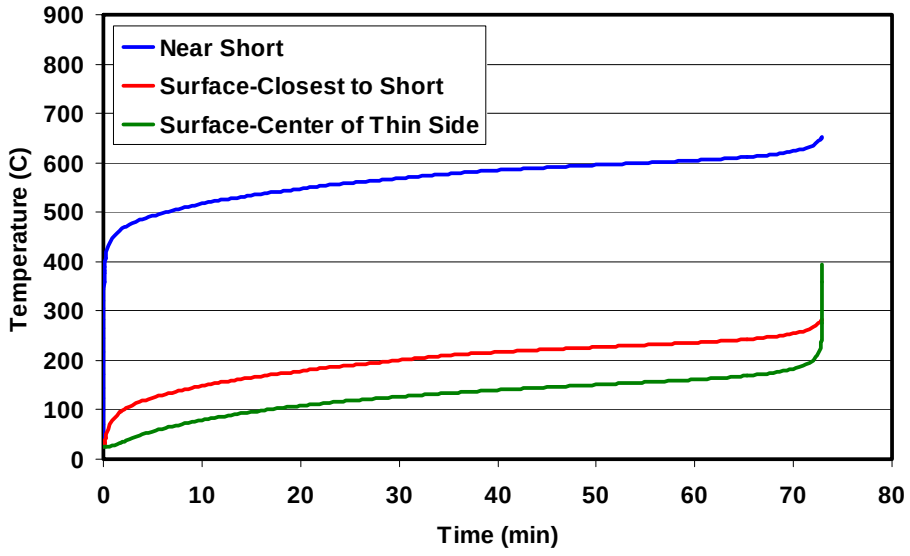

Figure 36: History of temperature versus time for three points in the cell: (1) near the short; (2) on the surface of the cell at the center of the large side (closest point to the short); and (3) at the surface of the cell at the center of its small side, for a primary short power of 75 W, with no secondary short power.

7.3.2. Very Low Secondary Short Power

If the secondary short power is distributed throughout the stack instead of being localized in the vicinity of the primary short, then the threshold value of the primary power for runaway is about 65 W. The threshold power for this condition is only 10 W less than when there is no secondary short at all. The reason for this higher threshold power is that, when the heat generation of the secondary short is distributed throughout the jellyroll, the jellyroll heats up more uniformly, and by the time a significant fraction of the jellyroll is hot enough to produce sizable decomposition reactions in the anode and cathode, the secondary short power dissipation in these regions is cut off by separator shutdown. Such behavior is illustrated in Figure 37, which shows the heat dissipation rates for a scenario in which the primary short power is only 60 W and the cell does not runaway. As is evident in the figure, the secondary short power is triggered almost immediately; however, over the next 10 minutes, the increase in heat generation due to anode decomposition is balanced by a decrease in the secondary short power arising from separator shutdown. Then, over the subsequent 10 minutes, the overall power continues to decrease as power in the short decreases due to separator shutdown, and the heat generation in the anode and cathode stay about the same. The overall power eventually decreases to a steady-state of about 69 W, with most of the separator shut down.

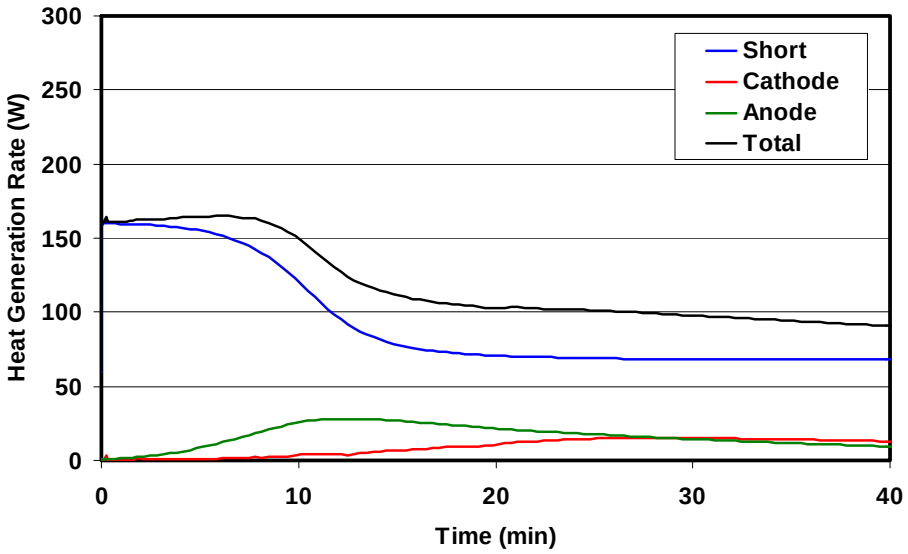

Figure 37: Heat generation rate versus time for: the short (both the initial and hard short); decomposition of the cathode; decomposition of the anode; and the sum of all three components for an initial short power of 60 W, with hard short power distributed throughout that part of the jellyroll in which the separator has not shut down.

7.3.3. Higher Secondary Short Power

We evaluated two different values for the case of higher secondary short power — 200 W and 1000 W. If the secondary short power increases to 200 W, then threshold power decreases from 22 W to 19 W. We don't expect further significant decrease in the threshold power with an increase in the secondary short power. However, the time for runaway depends strongly on the

secondary short power. Figure 38 shows the cell surface temperature for thermal runaway of the PHEV cell with a primary short power of 20 W and a secondary short power of 1 kW. As indicated earlier, recent work at TIAX in a separate project has shown that the Li-ion battery electrodes are capable of supporting very high short-term power values (higher than is generally appreciated in the literature) and so the secondary short power of 1kW is possible.

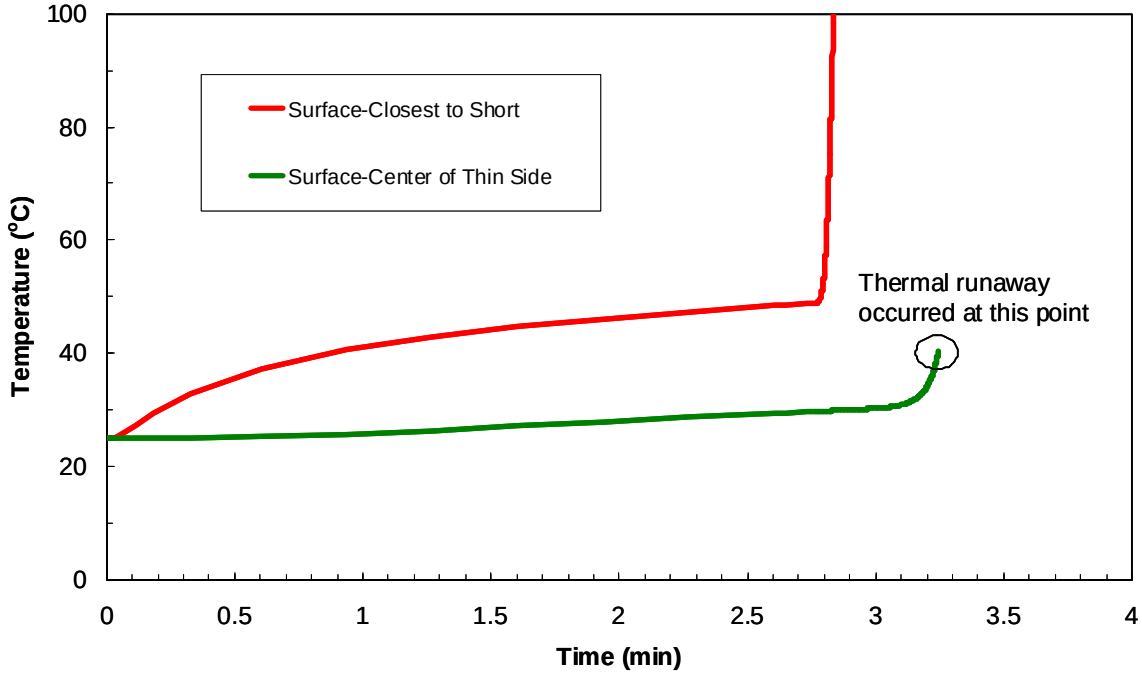

Figure 38: History of temperature versus time for two points in the cell: (1) on the surface of the cell at the center of the large side (closest point to the short); and (2) at the surface of the cell at the center of its small side, for a primary short power of 22 W, and secondary short power value of 1kW.

The results in Section 7.3, when taken together, illustrate the importance of the secondary short power in dictating conditions and likelihood of thermal runway. The factors that control the secondary short power must be further studied through experiments and simulations for more robust understanding of the factors that govern thermal runaway from internal shorts. There are likely very important implications for separator designs that might provide heightened protection.

7.4. FEA Results: Sensitivity to Cell Design or Environmental Parameter Modifications

In this section, we summarize the effects of cell design or environmental parameter modifications on the propensity for thermal runaway. These include the effect of:

- Changing the cell aspect ratio while keeping the same cell capacity of 33 Ah;
- Separator shut down;
- Doubling anode heat release kinetics;
- Doubling cathode heat release kinetics;
- Thicker current collectors.

7.4.1. Effect of aspect ratio

When the cell aspect ratio (surface area to volume) is modified so that the stack thickness is doubled and the planar area of the stack is decreased by 50% (keeping the volume of the stack the same and keeping the thickness of the insulator and can the same), the threshold power increases slightly, from 22 W to 24W. This small increase is due to the greater ability of the thicker cell to take heat away from the region of the short. In other words, the dissipation of heat through conduction is greater than it is through surface convection for the threshold condition.

In other conditions (i.e., primary short power greater than the threshold value), it is likely that the smaller surface-to-volume ratio will limit the amount of heat that can be removed from the cell, in which case this lower aspect ratio design may not be as effective.

7.4.2. Separator shut down

When the separator does not shut down, so that no cut-back in secondary short power can occur when the temperature reaches 130ºC, the threshold power decreases from 22 W to 19 W, indicating that separator shut down has only a modest influence on the propensity for thermal runaway.

7.4.3. Anode heat release kinetics

When the anode decomposition specific energy is decreased proportionally by 50% (i.e., all four reaction specific energies are cut by 50%), the threshold power increases from 22 W to 40 W. The basis for this simulation is the observation in experimental studies at TIAX that the morphology of the anode materials and the use of SEI-stabilizing additives can significantly reduce the heat release kinetics from the anode. However, the cathode heat release kinetics can be influenced only by changes to the active material itself.

7.4.4. Cathode heat release kinetics

When the heat release from the cathode is doubled, the threshold primary short power decreases a little, from about 22 W to about 20 W. If the primary short power is not sufficient to cause separator melting (primary short power of 18 W or less), then the cathode heat release is insignificant, and it has no bearing on cell behavior. However, once the secondary short is initiated and the temperature near the short increases substantially, the additional heat release from the cathode does contribute to runaway, so a lower primary short power is required to cause runaway.

7.4.5. Thicker current collectors

If the thickness of the current collectors is doubled, the in-plane and through-thickness effective thermal conductivity of the cell increases. The through-thickness thermal conductivity, which is limited more by the electrolyte-soaked anode, cathode and separator layers, increases by only about 10%, but the in-plane thermal conductivity increases by about 80%. The increase in thermal conductivity causes the primary short power required to melt the separator and initiate the secondary short to increase by several watts, from about 20 W to about 27 W reflecting a greater rate of heat transfer out from the cell. Once the secondary short of 100 W is initiated, the key parameter becomes the total power from both the primary and secondary shorts. Results

indicate that the total short power required to initiate runaway increases from 122 W to about 165 W, with a corresponding increase in primary short power from 22 W to 65 W.

7.5. Summary of FEA Simulations for PHEV-Sized Cells

The FEA model for the PHEV cell reveals several interesting trends that influence the propensity for thermal runaway:

- In general, mostly because of its greater size, but also because of its shape and the relative thermal conductivity in the stack with respect to this shape, the threshold power for a 33 Ah PHEV cell is substantially greater than the threshold power for an 18650 cell with the same characteristics and for the same environment. However, as measured in terms of c-rates, the threshold power for the larger PHEV cell is much smaller than for the 18650 cell.
- The estimated threshold power for runaway is greatly influenced by both the magnitude and the distribution of heat release from the secondary short. As discussed above, given the importance of this secondary short power in determining the propensity for runaway, additional experimental and simulation work needs to be undertaken to determine the factors that control this secondary power dissipation.
- Once the primary short power attains a critical value, the incremental change in the threshold power with respect to a further increase in the secondary power becomes smaller; in these cases, it is the primary short power that is required to activate the secondary short (i.e., the power from the initial short) that becomes the primary determinant of thermal runaway, because once the secondary short is activated, runaway is sure to occur. The time at which the runaway occurs may be significantly affected by the size of the secondary short, but otherwise the inevitability of a thermal runaway is not changed. Given the stochastic nature of the secondary short power value, and hence the time for thermal runaway to occur, it is imperative to detect internal short circuits as soon as is possible so that intervention measures can be activated.
- The shutdown of the separator has only a modest influence on the threshold power for runaway.
- It appears that large (obviously transient) gradients in temperature can be present in the PHEV cell, even when it is not running away. A more thorough investigation of anode/cathode exothermic kinetics that may occur above 350 ºC is necessary because such temperatures will arise near the short in some cases where the cell reaches a steady-state and does not run away, and decomposition heat rates are typically not captured in DSC measurements.
- The characteristics of the anode and cathode materials, and in particular their exothermic heat release rates, also affect the threshold power significantly, but typically not as strongly as surface heat transfer conditions. However, if the separator does not shut down and the secondary short power is sufficiently high, the kinetics of decomposition play only a minor role in determining threshold power.

8. Conclusions and Recommendations: Implications for PHEV pack design

The body of work carried out in this project has significantly advanced our knowledge of the parameters that determine thermal runaway in a Li-ion cell. The ability to fabricate custom-designed cells and test them under controlled external heat transfer conditions has proved critical in gaining this knowledge. We believe that simulation of thermal runaway of Li-ion cells in the literature has been hampered by the lack of access to well-characterized data. However, the tools and the other methodologies developed in this project have allowed the calibration of an FEA model for simulating thermal runaway of Li-ion cells and understanding progression of an internal short to a thermal runaway.

A major conclusion from this work is that the cell-surface and internal rates of heat transfer have a major impact on the propensity for thermal runaway of Li-ion cells. Simulation of thermal runaway of PHEV cells using our FEA model with calibrated parameters shows that the external heat transfer coefficient plays a crucial role in determining whether thermal runaway occurs following an internal short circuit. In the end, the propensity for runaway relates to conditions for which the rate of heat generation inside the cell due to the primary and secondary shorts and the electrode decomposition reactions persists at values greater than the rate of heat removal from the cell through surface convection and radiation, and through other, less desirable means, such as venting and expulsion of hot gas. Increasing the effective surface heat transfer rate not only increases the rate of heat removal, but also limits the rate of heat generation due to formation of secondary shorts and decomposition of the electrode materials.

Another approach to increased effectiveness of heat transfer from the cell is to increase the aspect ratio, that is, increase the surface to volume ratio of the cell. Essentially, cells that are thinner with greater surface area will be able to shed heat faster from the surface and hence reduce the propensity for thermal runway. However, this benefit of the aspect ratio must be balanced with vehicle design constraints that may not allow infinite flexibility in cell design and placement.

The impact of the internal and external heat transfer rates on propensity for thermal runaway also suggests that the most likely condition for thermal runaway would depend on the cooling system design. In battery packs with active cooling systems, the most dangerous condition is when the pack is fully charged and at rest and the cooling system is turned off. Under these conditions, the surface heat transfer coefficient will be at its lowest value. A potentially “dangerous” internal short that forms under these conditions can quickly result in thermal runaway of the cell.

The results in this work also point to the importance of controlled heat transfer conditions in studying thermal runaway of Li-ion cells. Frequently, in laboratory tests such as the hot box test or the overcharge test, the external heat transfer condition is not controlled. This lack of control can clearly lead to erroneous conclusions when comparing different types of cells or materials with respect to their propensity for thermal runaway. For example, the heat transfer conditions are not specified for standardized safety tests such as the overcharge test. Therefore, if the heat transfer rate changes from 12 to 20 W/m^2-K in an overcharge experiment comparing cells with two different sets of active materials —which represents just a modest increase in the air flow rate around the cell — then the cells tested at the higher heat transfer rate will appear to be safer in these tests primarily because of the increased heat transfer rate, and not because of any inherent differences in the stability of the active materials.

The results in this work highlight the importance of early detection of the primary internal short so that suitable intervention techniques can be deployed in preventing thermal runaway. Essentially, the time to thermal runaway is highly stochastic, especially when it is determined by the nature of the secondary shorts that are created. Early detection allows for early deployment of intervention methods therefore ensuring a better chance of preventing thermal runaway.

Increasing the internal conductivity of the cell can also enhance the safety of Li-ion cells to the internal short trigger. Simulations show that increasing the internal rate of heat transfer by increasing the thermal conductivity of the cell components can enhance resistance to thermal runaway for an internal short trigger. These results are consistent with the anecdotal evidence that increasing the current collector thickness can improve the safety of Li-ion cells in standardized tests.

The separator characteristics have a major influence on the propensity for thermal runaway. Separator melting, which induces a secondary short in the vicinity of the primary short, appears to be important in determining the internal short threshold power value. However, the nature of the secondary short that ensues from separator melting appears to be extremely stochastic. The time for progression to thermal runaway from the secondary short formation is also, therefore, stochastic. The nature of the secondary short that forms from separator melting must be studied in greater detail. For example, does the nature of the short depend on the local electrode morphology? Does the short power depend on the local stack pressure? Do ceramic layers on the separator really influence the nature of this secondary short that forms when the separator melts?

Whether or not the kinetics of the anode/cathode decomposition reactions have a major influence on the propensity for thermal runaway depends on the secondary short power and external heat transfer conditions. Experimental work at TIAX has indicated that the use of lower-surface area anode material and the use of SEI-stabilizing additives can significantly improve the thermal stability of the anode. Such improvements would appear to significantly increase the threshold power for thermal runaway.

The body of work completed in this project highlights the complicated phenomena underlying thermal runaway of Li-ion cells and raises significant questions that must be further studied through experiments and simulations:

- Improved understanding of separator shut down and melt characteristics and the nature of the secondary shorts that form subsequent to separator melting.
- Mathematical representations of the kinetics of exothermic heat release from the anode and cathode decomposition reactions that are derived from fundamental mechanistic studies so that they can be used over a wide range of conditions.
- Related to the above point are improved techniques for characterization of the thermal decomposition kinetics of anode and cathode reactions. Conventional approaches include use of DSC or ARC measurements. However, these methods are not standardized, and do not accurately reflect the conditions within a cell. For example, what is the correct electrolyte to active material ratio to be used in these tests (especially given the very large quantity of energy associated with potential electrolyte decomposition)?
- The importance of pressure rise within the cell when the temperature rises with the cell. When will the pressure rise in the cell be sufficient to vent the cell so as to prevent thermal

runaway? Should greater efforts be applied to engineering vent designs that incorporate pre-emptive termination of a developing thermal runaway?

Bibliography

[1] "Mitsubishi reports fire in i-MiEV battery pack, melting in Outlander PHEV pack," Japan Times, March 27, (2013)

[2] B.Barnett, D.Ofer, S.Sriramulu, R. Stringfellow, "*Safety Issues in Li-Ion Batteries*" in: Robert A. Meyers (Ed.), Encyclopedia of Sustainability Science and Technology, Springer Science, 2012.

[3] B. Barnett, S. Sriramulu, "A Perspective on Li-Ion Safety and Opportunities for Portable and Electric Vehicle Applications", Presentation at the 27th International Battery Seminar & Exhibit, Ft. Lauderdale, Florida (2010);

[4] R. Stringfellow, D. Ofer, S. Sriramulu, and B. Barnett, New Framework for Lithium-Ion Battery Safety, IMLB, Montreal, Canada, Invited Talk (TIAX LLC) (2010); "Perspective on Mitigating Safety Incidents in Li-Ion Cells", Suresh Sriramulu, Surendra K. Singh, Richard Stringfellow, David Ofer, Bookeun Oh, Brian Barnett, 43rd Power Sources Conference, Philadelphia, PA (2008); "Influence of active material heat release kinetics on thermal runaway following an internal short-circuit," S.K. Singh, R. Stringfellow, B. Barnett, S. Sriramulu, 212th Meeting of the Electrochemical Society, Washington, D.C. (2007).